


Summer 8-7-2015

Individual Tree Measurements From Three-Dimensional Point Clouds

Elias Ayrey

University of Maine - Main, elias.ayrey@maine.edu

Follow this and additional works at: <http://digitalcommons.library.umaine.edu/etd>

 Part of the [Biometry Commons](#), [Forest Biology Commons](#), [Forest Management Commons](#), and the [Other Forestry and Forest Sciences Commons](#)

Recommended Citation

Ayrey, Elias, "Individual Tree Measurements From Three-Dimensional Point Clouds" (2015). *Electronic Theses and Dissertations*. 2284.
<http://digitalcommons.library.umaine.edu/etd/2284>

This Open-Access Thesis is brought to you for free and open access by DigitalCommons@UMaine. It has been accepted for inclusion in Electronic Theses and Dissertations by an authorized administrator of DigitalCommons@UMaine.

**INDIVIDUAL TREE MEASUREMENTS FROM
THREE-DIMENSIONAL POINT CLOUDS**

By

Elias Ayrey

B.S. Binghamton University, 2012

A THESIS

Submitted in Partial Fulfillment of the

Requirements for the Degree of

Master of Science

(in Forest Resources)

The Graduate School

The University of Maine

August 2015

Advisory Committee:

Shawn Fraver, Assistant Professor of Forest Ecosystems, Advisor

Brian Roth, Assistant Director of the Cooperative Forestry Research Unit

Aaron Weiskittel, Associate Professor of Forest Biometrics and Modeling

THESIS ACCEPTANCE STATEMENT

On behalf of the Graduate Committee for Elias Ayrey, I affirm that this manuscript is the final and accepted thesis. Signatures of all committee members are on file with the Graduate School at the University of Maine, 42 Stodder Hall, Orono, Maine.

Dr. Shawn Fraver, Assistant Professor of Forest Ecosystems

Date

LIBRARY RIGHTS STATEMENT

In presenting this thesis in partial fulfillment of the requirements for an advanced degree at the University of Maine, I agree that the Library shall make it freely available for inspection. I further agree that permission for "fair use" copying of the thesis for scholarly purposes may be granted by the Librarian. It is understood that any copying or publication of this thesis for financial gain shall not be allowed without my written permission.

Signature:

Date:

INDIVIDUAL TREE MEASUREMENTS FROM THREE-DIMENSIONAL POINT CLOUDS

By: Elias Ayrey

Thesis Advisor: Dr. Shawn Fraver

An Abstract of the Thesis Presented
in Partial Fulfillment of the Requirements for the
Degree of Master of Science
(in Forest Resources)
August 2015

This study develops and tests novel methodologies for measuring the attributes of individual trees from three-dimensional point clouds generated from an aerial platform. Recently, advancements in technology have allowed for the acquisition of very high resolution three-dimensional point clouds that can be used to map the forest in a virtual environment. These point clouds can be interpreted to produce valuable forest attributes across entire landscapes with minimal field labor, which can then aid forest managers in their planning and decision making.

Biometrics derived from point clouds are often generated on a plot level, with estimates spanning many meters (rather than at the scale of individual the individual tree), a process known as area-based estimation. As the resolution of point clouds has increased however, the structural attributes of individual trees can now be distinguished and measured, which allows for tree lists including species and size metrics for individual trees. This information can be of great use to forester managers; thus, it is essential that proper methods be developed for measuring these trees.

To this end, an algorithm called *layer stacking*, was developed to isolate points representing the shapes of individual trees from a Light Detection and Ranging (LiDAR)

derived point cloud, a process called segmentation. The validity of this algorithm was assessed in a variety of forest stand types, and comparisons were made to another popular tree segmentation algorithm (i.e., watershed delineation). Results indicated that when compared to watershed delineation, layer stacking produced similar or improved detection rates in almost all forest stands, and excelled in deciduous forests, which have traditionally been challenging to segment.

The algorithm was then implemented on a large scale, for individual measurements on over 200,000 trees. The species and diameter of each tree was predicted *via* modeling from structural and reflectance characteristics, and allometric equations were used to obtain volume and carbon content of each tree. These estimates were then compared to measurements taken in the field, and to area-based estimates. Results indicated improved accuracy of plot level basal area, volume, and carbon estimation over traditional area-based estimation, as well as moderately reliable individual tree estimates, and highly reliable species identification.

Finally, because LiDAR point clouds can be expensive to acquire, point clouds generated from aerial photos *via* structure-from-motion (SfM) reconstruction were evaluated for their accuracy at a tree level. An analysis between tree height measurements obtained by SfM, SfM in conjunction with LiDAR, LiDAR alone, digital stereo-photo interpretation, and field measurements was conducted. Results indicated no difference between SfM in conjunction with LiDAR and LiDAR alone. We concluded that SfM represents a valid low cost means of producing a point cloud dense enough to measure individual trees.

Thus, high resolution point clouds can be used to generate forest inventories containing a number of valuable biometrics, such as tree height, species, volume, biomass, and carbon mass. Such estimates may allow for the automatic development of large-scale, detailed, and precise forest inventories without the cost, effort, and safety concerns associated with extensive field inventories.

ACKNOWLEDGMENTS

I'd like to thank my graduate advisor, Shawn Fraver, for introducing me to this topic of which I am so impassioned, as well as providing me with invaluable assistance at each step throughout the program. He made himself constantly available to help with problems big and small, and I have no doubt my career would be taking a very different path were it not for him.

I'd like to thank Brian Roth for his help with data collection, and his unending flow of new ideas. I'd like to thank Aaron Weiskittel for helping me through the rough patches with his vast statistical expertise. I also thank Laura Kenefic for her assistance with data collection and revisions, as well as for a particular motivational email early in my career.

Data for this study was collected by the U.S. Forest Service's Northern Research Station with the help of Laura Kenefic and Nicole Rogers, by University of Maine's Cooperative Forestry Research Unit with the help of Brian Roth, and by NASA Goddard's G-LiHT program with the help of Bruce Cook.

Finally, I'd like to thank my father, Robert Ayrey, who has done more to further my education than anyone else. As well as my grandfather, Dr. David Falk, whose scientific career serves as a personal inspiration.

TABLE OF CONTENTS

ACKNOWLEDGMENTS.....	iii
LIST OF TABLES.....	vii
LIST OF FIGURES.....	viii
CHAPTER ONE: LAYER STACKING: A NOVEL ALGORITHM FOR INDIVIDUAL FOREST TREE SEGMENTATION FROM LIDAR POINT CLOUDS.....	1
Introduction.....	1
Methods.....	4
Study Area.....	4
LiDAR Acquisition.....	7
Tree Detection.....	7
Tree Segmentation.....	12
TIFFS Watershed Delineation.....	14
Verification.....	14
Results.....	15
Discussion.....	19
Conclusions.....	23

CHAPTER TWO: DETERMINATION OF INDIVIDUAL TREE SPECIES,
DIAMETER, VOLUME, AND CARBON STOCK FROM AIRBORNE LIDAR FOR
LARGE-SCALE STAND INVENTORIES IN MIXED SPECIES FORESTS.....25

 Introduction.....25

 Methods.....29

 Study Area.....29

 LiDAR.....29

 Individual Tree Segmentation.....30

 Individual Tree Measurements.....31

 Species Identification.....34

 Individual Tree Diameter Estimation.....35

 Individual Tree Stem Volume.....35

 Individual Tree Aboveground Carbon.....36

 Post-hoc ITC Correction.....36

 Area-Based Estimation.....36

 Biometric Validation.....37

 Results.....40

 Segmentation.....40

Species Identification.....	41
Tree Level Validation.....	43
Plot Level Validation.....	45
Stand Level Validation.....	49
Discussion.....	49
Conclusion.....	55
CHAPTER THREE: THREE-DIMENSIONAL POINT CLOUD RECONSTRUCTION FROM AERIAL PHOTOS AS A MEANS OF ESTIMATING INDIVIDUAL TREE HEIGHT IN CONIFER STANDS.....	
	57
Introduction.....	57
Methods.....	60
Results and Discussion.....	66
EPILOGUE.....	71
Summary of Chapters.....	71
The Future of Point Cloud Technology.....	73
REFERENCES.....	76
APPENDIX A: METHODS OF TREE CROWN MEASUREMENT.....	84
BIOGRAPHY OF THE AUTHOR.....	85

LIST OF TABLES

Table 1.1: Stand characteristics of the study area.....	6
Table 1.2: Detection rates of layer stacking and watershed delineation.....	16
Table 2.1: Tree measurements used for modeling.....	32
Table 2.2: Stand characteristics of the study area.....	39
Table 2.3: Detection rates by stand and forest type.....	41
Table 2.4: Species classification confusion matrix.....	43
Table 2.5: Plot level volume estimates and biases.....	48
Table 3.1: Summary statistics for each species measured.....	62
Table 3.2: Mean biases and absolute differences between measurement methods.....	68

LIST OF FIGURES

Figure 1.1: Workflow of the layer stacking tree detection algorithm.....	9
Figure 1.2: Comparison between layer stacking and density of high points.....	11
Figure 1.3: Portions of the layer stacking tree segmentation algorithm.....	12
Figure 1.4: Detection rate displayed by stem diameter.....	19
Figure 1.5: Comparison of results between layer stacking and watershed delineation.....	22
Figure 2.1: Tree level comparisons between field measurements and LiDAR estimates.....	44
Figure 2.2: Plot level comparisons between field measurements, layer stacking, and area based estimates.....	46
Figure 3.1: A structure-from-motion point cloud overlaid on top of a LiDAR point cloud.....	65
Figure 3.2: Mean tree height by species and measurement method.....	67
Figure A1: Methods of tree crown measurement.....	84

CHAPTER ONE:

LAYER STACKING: A NOVEL ALGORITHM FOR INDIVIDUAL FOREST TREE SEGMENTATION FROM LIDAR POINT CLOUDS

Introduction

Current advances in remote sensing are improving the accuracy and scope of forest inventories by using high resolution three-dimensional spatial data. One of the most effective tools for retrieving such data is Light Detecting and Ranging (LiDAR), which uses laser range finding to create three-dimensional point clouds representing forest canopy structure. Aerial LiDAR applications for forest inventories can be divided into two categories. First, *area-based* approaches retrieve general height metrics such as mean point height and point height distributions. These data are used to estimate, for example, forest volume, biomass, and stem density through regression and other modeling techniques (Means et al. 2000, Næsset 2002, Maltamo et al 2004). Second, *individual-tree-based* approaches first retrieve detailed metrics from individual trees (often directly measuring each tree's crown attributes), then either aggregate them to characterize forest attributes for larger areas, or use them in combination with area-based approaches (Lindberg 2010).

Area-based approaches have been more widely employed than individual-tree approaches, in part because most LiDAR datasets have point densities considered too sparse for the identification of individual tree crowns from point clouds, a process referred to as *segmentation*. However, densities of LiDAR data collections are rapidly improving, with collections regularly flown at a density of ten or more pulses per square meter (pls/m²), making individual tree segmentation a feasible alternative to area-based

approaches. This opens the possibility for identifying and retrieving measurements from all canopy trees over large areas. Some benefits to the individual tree approach include: making the inventory more intuitive (i.e., closely resembling traditional field-based forest inventories but at much larger scales), easier classification of tree species (Vastaranta et al. 2009), and more precise inventories that include listed attributes of each tree.

Previous segmentation endeavors show promise, yet still highlight the challenge of isolating individual trees. For example, in a comparison across segmentation methods, Vauhkonen et al. (2011) reported individual tree detection rates (defined as percent of trees correctly detected) ranging between 40 and 80% across a variety of forest types. In a similar study, Kaartinen et al. (2012) reported a range between 40 and 90% with boreal conifers. Because of this challenge and variability, few studies have directly compared area-based and individual-tree approaches. Yu et al. (2010) conducted such a comparison and found that the two approaches produced comparable mean tree diameters, heights, and volumes, but concluded that the individual-tree approach may yield better results with improved segmentation methods.

Several segmentation methods are currently available, the most commonly used being watershed delineation and its variants. This method proceeds by creating a model of the canopy surface (referred to as a canopy height model, CHM), which is inverted to reveal the local maxima ridges that delineate adjacent individual tree crowns (Soille 1999, Chen et al. 2006, Kwak et al. 2007). The method yields favorable results in stands of uniform crown shapes, with distinct peaks and troughs, such as pure even-aged conifer stands; it performs less well when applied to more complex or interlocking crowns, such as those of deciduous stands (Koch et al. 2006). Although standard watershed

segmentation, along with other CHM-based segmentation algorithms, are unable to detect overtopped trees (Koch et al. 2014), several variations of watershed delineation show promise in detecting overtopped trees by examining the point cloud beneath the canopy surface (Reitberger et al. 2009, Duncanson et al. 2014).

While watershed segmentation is currently the most popular method, others are sometimes applied. The local maxima method identifies the peaks of tree crowns and delineates a surrounding crown area by expanding outward from those peaks in a variety of ways, such as valley following or seeded region growing (Wulder et al. 2000, Perrson et al. 2002, Popescu et al. 2002, Popescu et al. 2004). The density of high points method introduced by Rahman and Gorte (2009) creates a model, analogous to that of a CHM used in watershed delineation, based on the density of points. Clustering algorithms are also often applied to segmentation, with k-means or hierarchical clustering being the most common (Morsdorf et al. 2003, Gupta et al. 2010, Lee et al. 2010). Both show promise for isolating individual trees; however, k-means clustering requires prior knowledge of the number of trees present, and hierarchical clustering requires user input or the same knowledge of trees present to decide a stopping point for the clustering process. A further limitation arises when the densest point clusters (assumed to represent the tree center) occur where adjacent crowns interlock.

We present a novel segmentation algorithm referred to as *layer stacking* that attempts to overcome several of the challenges faced by the algorithms outlined above. Layer stacking involves slicing the forest canopy into horizontal layers, clustering points within each layer, then stacking the layers to assess cluster location agreements that emerge among layers. The centers of areas of greater agreement are taken to represent the

centers of individual trees. The algorithm builds upon concepts implemented in clustering segmentation (Gupta et al. 2010), density of high points scanning (Rahman and Gorte 2009), and local maxima detection algorithms (Popescu 2002). We tested the ability of layer stacking to detect trees by applying it to LiDAR for which we had field-mapped and measured tree data representing a range of tree species compositions and structures. We also tested layer stacking against a commercially available watershed algorithm using these same plots.

Methods

Study Area

To assess the accuracy of layer stacking, sites were needed that had a variety of forest stand structures and compositions as well as accurate field-measured tree heights and mapped locations for many individual trees. The sites we selected were located in Maine and New Brunswick's mixedwood Acadian Forest, which support nearly pure coniferous stands similar in structure to boreal forests in northern latitudes, pure deciduous stands similar in structure to the temperate forests of the Mid-Atlantic region, and various mixtures of the two. Three sites were used for algorithm verification. The first was the University of Maine Foundation's Penobscot Experimental Forest (PEF, at 44.879, -68.653), chosen for the even- and uneven-aged silvicultural treatments applied there by the U.S. Forest Service, Northern Research Station. The second was the University of Maine's Cooperative Forestry Research Unit's Austin Pond (AP, at 45.199, -69.708) study, chosen for its even-aged silviculture. The third was the University of New Brunswick's Noonan Research Forest (NRF, at 45.988, -66.396), chosen for its mixedwood forest.

Plots used for verification had previously been established at each site. Plots on the PEF were fixed-radius plots of either 15.9 or 20 m, plots at AP were 30 × 25 m, and plots at Noonan were 50 × 50 m. Plot centers were taken via GPS, and then were shifted *a posteriori* to align the trees visually with the raw LiDAR point clouds. Trees greater than 11.4 cm diameter at breast height (DBH, 1.37 m) at the PEF and 10 cm DBH at AP and NRF were plotted spatially, with height and species also noted. Table 1.1 lists the attributes and background of each stand. Species composition was noted as the relative frequency of each tree species for plotted trees, and reported down to 5%. Plots with greater than 400 trees per ha were considered to be 'dense', while those with less were considered as 'sparse'. By this designation, the AP site had a high density of trees; however, the uniform tree spacing resulting from pre-commercial thinning, similar to that of a plantation, resulted in different algorithm performance from the other dense even-aged plots. For this reason, this plot was placed in a separate category.

Table 1.1 Stand characteristics of the study area. Includes silvicultural history, species composition, and year measured for the 11 stands under study. Stands are grouped by forest type. Stand metrics were based on trees greater than or equal to 11.4 cm DBH. The sites included Penobscot Experimental Forest (PEF), Austin Pond (AP), and Noonan Research Forest (NRF).

Stand Identifier	Density (trees/ha)	Basal Area (m ² /ha)	Silvicultural Treatment	Species Composition*	Year Inventoried	Number of Plots
Dense uneven-aged conifers						
PEF-9	510 ± 37	29.2 ± 1.2	Single-tree selection system. Last harvested 2010	35% <i>Abba</i> , 33% <i>Tsca</i> , 14% <i>Piru</i> , 9% <i>Acru</i>	2013	4
PEF-16	509 ± 24	25.6 ± 2.1	Single-tree selection system. Last harvested 2012	39% <i>Tsca</i> , 38% <i>Abba</i> , 9% <i>Piru</i> , 7% <i>Acru</i>	2011	6
PEF-12	617 ± 27	28.1 ± 1.7	Single-tree selection system. Last harvested 1995	52% <i>Abba</i> , 18% <i>Tsca</i> , 14% <i>Acru</i> , 9% <i>Piru</i>	2014	5
PEF-28	564 ± 13	22.9 ± 2.5	Modified diameter limit cutting. Last harvested 1997	43% <i>Abba</i> , 18% <i>Tsca</i> , 15% <i>Acru</i> , 12% <i>Piru</i>	2007	4
Sparse uneven-aged conifers						
PEF-15	319 ± 12	7.5 ± 0.7	Fixed diameter-limit cutting. Last harvested 2003	39% <i>Abba</i> , 26% <i>Tsca</i> , 14% <i>Piru</i> , 9% <i>Acru</i> , 5% <i>Bepa</i>	2007	6
Dense even-aged conifers						
PEF-23B	1434 ± 50	30.3 ± 2.6	Uniform shelterwood, three-stage overstory removal	44% <i>Abba</i> , 31% <i>Pist</i> , 10% <i>Tsca</i> , 10% <i>Piru</i>	2011	3
PEF-29B	869 ± 29	17.3 ± 0.7	Uniform shelterwood, three-stage overstory removal	44% <i>Piru</i> , 25% <i>Abba</i> , 14% <i>Pist</i> , 5% <i>Bepo</i>	2011	3
Spaced even-aged conifers						
AP	1332	33.5	Clearcut, followed by pre-commercial thinning in 1983	79% <i>Abba</i> , 11% <i>Piru</i>	2014	1
Dense mixedwood						
NRF	1012	43.6	Naturally regenerated following fire	24% <i>Thoc</i> , 23% <i>Acru</i> , 23% <i>Piru</i> , 11% <i>Abba</i> , 6% <i>Beal</i> , 5% <i>Bepa</i>	2015	1
Sparse even-aged deciduous						
PEF-M1	337	21.5	Commercially thinned in 2011, reserve prior	62% <i>Acsa</i> , 7% <i>Acru</i> , 7% <i>Osvi</i> , 5% <i>Tiam</i> , 5% <i>Fram</i>	2015	1
Dense even-aged deciduous						
PEF-M2	608	45.3	Reserve	66% <i>Acsa</i> , 9% <i>Fram</i> , 7% <i>Osvi</i> , 5% <i>Tiam</i> , 5% <i>Frgr</i>	2015	1

*Species abbreviations are as follows: *Abba* = *Abies balsamea*, *Acru* = *Acer rubrum*, *Acsa* = *Acer saccharum*, *Beal* = *Betula alleghaniensis*, *Bepa* = *Betula papyrifera*, *Bepo* = *Betula populifolia*, *Fram* = *Fraxinus americana*, *Frgr* = *Fraxinus grandifolia*, *Osvi* = *Ostrya virginiana*, *Piru* = *Picea Rubens*, *Pist* = *Pinus strobus*, *Tiam* = *Tilia americana*, *Tsca* = *Tsuga canadensis*, *Thoc* = *Thuja occidentalis*

LiDAR Acquisition

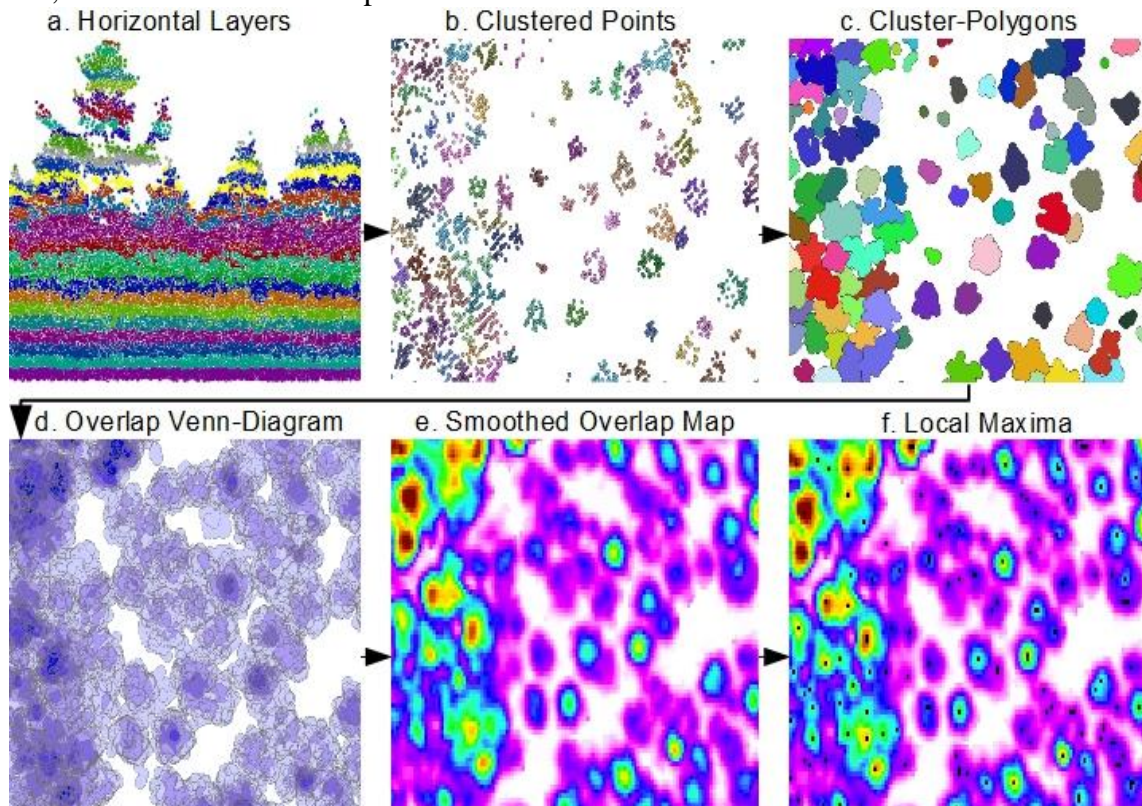
Three LiDAR datasets were collected. The first LiDAR acquisition took place in June, 2012, with NASA Goddard's LiDAR, Hyperspectral, and Thermal Imager (Cook et al. 2013) over the PEF at an average of 15 pls/m², with a pulse rate of 300 Khz, an average footprint size of 10 cm, a 28.5 degree maximum scan angle from nadir, and an altitude of approximately 335 m above ground level (AGL). The second LiDAR dataset was acquired over the PEF and AP in October, 2013, in leaf-off conditions with a RIEGL LMS-Q680i at an average of 6 pls/m², with a pulse rate of 150 Khz, an average footprint size of 0.17 m, a 28.5 degree maximum scan angle, and at an altitude of approximately 600 m AGL. The two PEF datasets were combined visually by aligning easily identified objects. This alignment appeared valid throughout the entire dataset, and trees were not shadowed or distorted. Thus the final average point density was ~ 21 pls/m² over the PEF, and ~ 6 pls/m² over AP. The third LiDAR dataset was collected at the NRF under a leaf-off condition in late October, 2011, using the same RIEGL LMS-Q680i laser scanner. The mean flying altitude was 724 m AGL and the maximum scan angle was 28.5 degrees. All LiDAR was collected at a 1550 nm wavelength. Ground points were classified by the provider.

Tree Detection

Before segmentation could proceed, we first had to detect the centers of all trees within the stands in question. Raw LiDAR data were first normalized to measure absolute height above ground by subtracting all points from a digital terrain model (DTM) derived from ground points. Individual forest stands were then separated using a pre-defined stand map. Each stand was segmented in its entirety including the plots within.

Each stand selected for segmentation was first horizontally layered at one-m intervals starting at 0.5 m above the ground and continuing to the highest point (Fig. 1.1a). Clustering algorithms were then applied to each layer. To filter out potentially unwanted low vegetation, the lowest three layers were first subjected to Density Based Scanning (DBScanning), as formulated by Ester et al. (1996). DBScanning classifies points into clusters based on a density and a minimum number of points per cluster as defined by the user. All points within clusters were thus classified as unwanted low vegetation and removed. All points outside of clusters were assumed to be solitary returns off the narrow tree boles, and were retained.

Figure 1.1: Workflow of the layer stacking tree detection algorithm. (a) Forest canopy is layered horizontally at 1-m intervals (side view). (b) Points in each layer are clustered; each cluster is assigned a random color (top-down view at 10m height). (c) Half-meter polygonal buffers are placed around each cluster. (d) Polygons from all layers are stacked on top of one another; areas with darker blue represent more overlap. (e) Areas of overlap between polygons from the different horizontal layers are rasterized and smoothed to produce an overlap map. Areas of increasing warmth (yellow and red) represent greater overlap. (f) Local maxima are detected from the overlap map, and displayed as black dots; these are assumed to represent the centers of trees.



Each layer was then subjected to agglomerative hierarchical clustering (Fig. 1.1b), utilizing the 'fastcluster' package in R (Müllner 2013), which generates a point-to-point distance matrix, based on horizontal Euclidean distance, and clusters the nearest points iteratively, repeating the process until every point is assigned to one cluster. The iteration at which the algorithm is terminated must be defined by the user. Had the number of trees been known in advance (rarely a practical option), the clustering could have been terminated once that number was achieved. Instead, several termination levels were

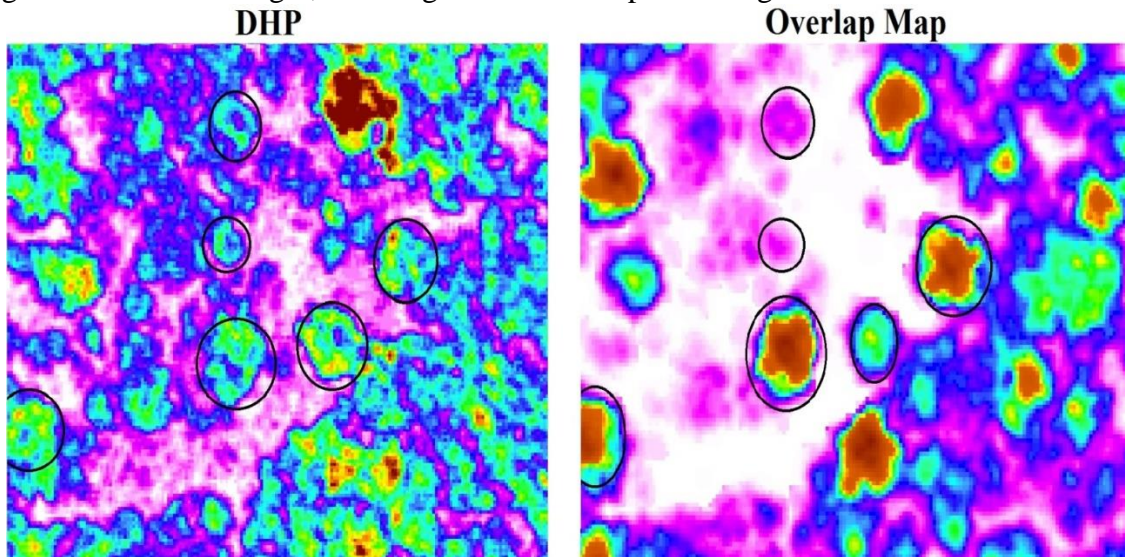
attempted, and a visual inspection of the resulting layers was conducted to determine which termination level best placed each tree into its own group. Attempts were made to automate the termination point based on number of points and perceived stand density, but large differences in canopy structure between stands made this infeasible.

Once points in each layer were optimally clustered, a 0.5 m polygonal buffer was placed around each cluster (Fig. 1.1c). This step served two purposes: first as an additional round of clustering because points further than 0.5 m from the main cluster, which may have been mistakenly placed into that cluster, were effectively separated from one another, and second as a means of connecting the points and vectorizing the clusters. When polygons overlapped in such a way as to form a complete ring around an empty interior, these ‘donut holes’ were filled, as they represented the centers of crowns where the laser could not penetrate. Each layer's polygons were then stacked (Fig. 1.1d), and a rasterized map of the number of overlapping polygons was generated with a resolution of 0.5 m.

In the same way a Venn diagram illustrates areas where two or more groups coincide, the overlap map identifies areas of high density in the canopy layers, such that multiple polygon overlaps indicate the presence of an individual tree. Double weight on the overlap map was given to clusters in the top third of the canopy, as they tended to represent tree apices and thus were closer to the tree's center. The overlap map is conceptually similar to the density of high points map developed by Rahman and Gorte (2009), except that the nature of the clustering, as well as the weighting applied to clusters in the upper layers, causes the hollow centers of hard-to-penetrate conifers to be

filled in, thus ensuring that the center of these trees truly have the most overlaps (Fig. 1.2).

Figure 1.2: Comparison between layer stacking and density of high points. A density of high points (DHP) map is displayed on the left, while an overlap map of a thinned conifer stand is displayed on the right. Both are smoothed. Areas of increasing warmth (yellow and red) represent higher values. Several trees are circled. Note that in the DHP map the trees form rings, with the areas of highest point density on the outside of the tree. On the overlap map the 'donut hole' rings are filled and the highest third of cluster-polygons are given double the weight, resulting in the densest point being at the center of the tree.



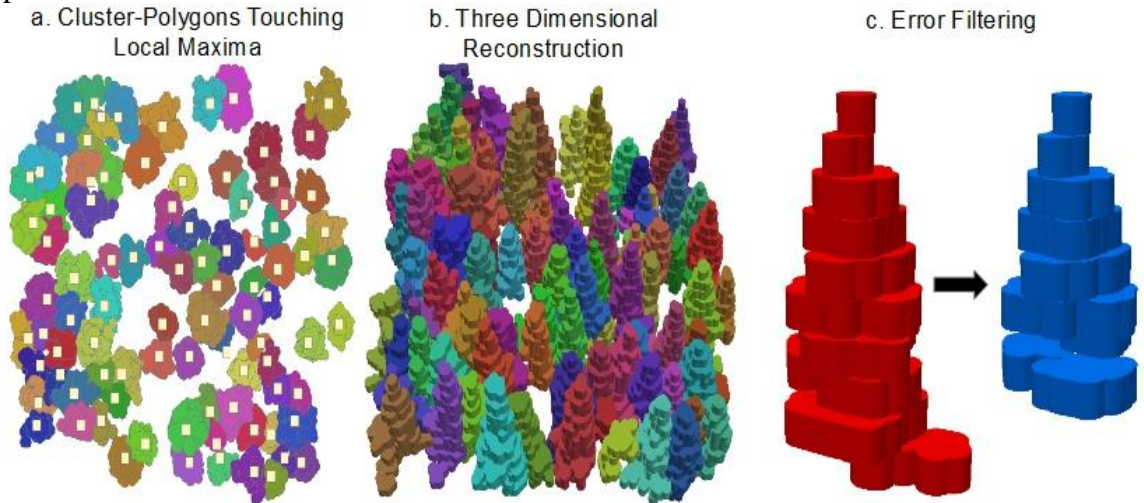
The overlap map was then smoothed, averaging cell values in a 3×3 cell window (Fig. 1.1e). This step was needed to remove areas of varying overlap within a tree that might represent branches, in the same way a CHM is smoothed prior to watershed delineation (Koch et al 2006). Local maxima were then detected with a 1-m fixed radius window (Fig. 1.1f). The local maxima detected then had to be filtered for errors. Those that rested atop an area with few overlapping clusters were removed, as they usually represented trees that were of an undesirably small size. Finally, local maxima that were closer than 1.5 m from one another (roughly the average crown radius across all plots on the PEF) were combined into a single tree. This step helped to prevent trees from being

incorrectly separated into multiple parts, though in very dense stands with small trees, it was beneficial to reduce this length threshold. The remaining local maxima were assumed to be the centers of trees and were then used for segmentation of individual tree shapes.

Tree Segmentation

Once tree centers were detected, a buffer of 0.6 m was placed around each local maxima. Our experience with these data sets and these tree species suggested that larger buffers would capture parts of neighboring trees, and smaller buffers would miss the furthest reaches of the crown. All cluster-polygons from each layer that intersected this buffered core were isolated as belonging to that local maxima's tree (Fig. 1.3a).

Figure 1.3: Portions of the layer stacking tree segmentation algorithm. This follows the tree detection steps shown in Figure 1. (a) Local maxima from the overlap map (Figure 1f) are used to delineate cluster-polygons that belong to trees. (b) Three-dimensional reconstruction of each tree's crown shape. (c) Error filtering eliminates mistaken clusters. Note the error filtering inadvertently removed some correct layers, causing a small portion of the tree's crown to be omitted.



Our algorithm includes three post-detection error-filtering steps to remove cluster-polygons that did not properly represent the shape of their respective tree. First, cluster-

polygons that intersected the cores of two trees were eliminated. It was hoped that this step would eliminate the canopy strata above overtopped trees, at the cost of slightly underestimating the size of the dominant tree's crown. Second, cluster-polygon areas so large as to be deemed outliers (generally greater than 2 absolute deviations when compared to other layers within that cluster's tree) were omitted, as these were assumed to represent the erroneous shapes of more than one tree. Third, cluster-polygons that only slightly overlapped the center of the tree, and had large areas, tended to be erroneous and often included parts of the neighboring tree's crown. Therefore, those cluster-polygons that overlapped the tree core area less than 10% and had abnormally large areas were removed (Fig. 1.3c). This area varied with tree height, given that taller trees could have larger crowns.

The remaining cluster-polygons associated with each tree were extruded three dimensionally back into their original layer so as to approximate the crown shape of each tree (Fig. 1.3b). The core of the tree, represented by the buffered local maxima, was also extruded to the height of the highest tree layer in order to ensure that points representing the tree bole were always captured, and not inadvertently removed in the filtering process. All points lying within these three-dimensional crown reconstructions (Fig. 3b) were then clipped out of the point cloud and assigned a unique tree identification. Three dimensional clipping was considerably faster with cubic features than with complex shapes; therefore, rectangular bounding boxes were placed around the cluster-polygons prior to the clip. The point clouds of each clipped tree were then combined back into one single point cloud for ease of verification.

TIFFS Watershed Delineation

We tested the efficacy of layer stacking against a popular watershed tree segmentation algorithm implemented in the Toolbox for LiDAR data Filtering and Forest Studies (TIFFS, Chen 2007). Raw LiDAR from each plot was input into TIFFS, and the shape of each delineated crown was used to clip points representing individual trees from the point cloud. Default settings were used in TIFFS, with the exception being that a 0.5 m fixed radius window was used to smooth the surface model.

Verification

Verification was conducted by comparing the two segmented point clouds, from the layer stacking and watershed algorithms, with locations of individually mapped trees from field-measured plots, which are taken as the reference for comparison. Points representing delineated trees from both algorithms were assigned random color values by tree number. Detection rates were assessed manually, tree by tree, with field measured trees plotted in three dimensional space as vertical columns extruded to the field measured height of the tree, and the LiDAR point clouds overlaid. Detection or omission of each tree was noted, and an overall tally of commission errors was made for each plot. Where multiple plots occurred in a stand, plots were summed by adding all detected and undetected trees in each plot together, along with commission errors, to produce a stand-level metrics.

Results

Results in the form of detection rate and commission error for both algorithms are displayed in Table 1.2 for each stand and forest type. Results varied dramatically from one forest type to another, and each algorithm performed optimally under different forest conditions

Table 1.2: Detection rates of layer stacking and watershed delineation. Trees detected by both the Toolbox for LiDAR Filtering and Forest Studies (TIFFS) watershed algorithm and by Layer Stacking is shown for each forest stand, along with detection rate (bold) and commission error. The sites included Penobscot Experimental Forest (PEF), Austin Pond (AP), and Noonan Research Forest (NRF).

Stand Identifier	Number of Trees Measured	TIFFS				Layer Stacking			
		Correctly Detected	Total Trees Segmented	Detection Rate	Commission Error	Correctly Detected	Total Trees Segmented	Detection Rate	Commission Error
Dense Uneven-Aged Conifers									
PEF-9	164	80	99	49%	12%	90	108	55%	11%
PEF-16	256	125	164	49%	15%	157	195	61%	15%
PEF-12	210	99	112	47%	6%	131	157	62%	12%
PEF-28	179	99	152	55%	30%	114	168	64%	30%
Sparse Uneven-Aged Conifers									
PEF-15	143	112	314	78%	141%	120	261	84%	99%
Dense Even-Aged Conifers									
PEF-23B	343	240	488	70%	72%	220	281	64%	18%
PEF-29B	211	152	304	72%	72 %	139	210	66%	34%
Spaced Even-Aged Conifers									
AP	123	91	123	74%	26%	91	106	74 %	12%
Dense Mixedwood									
NRF	253	110	154	43%	16%	134	180	53%	18%
Sparse Even-Aged Deciduous									
PEF-M1	61	33	54	54%	34%	52	83	85%	36%
Dense Even-Aged Deciduous									
PEF-M2	76	33	56	43%	30%	54	62	71%	10%

Layer stacking detected slightly more trees than watershed delineation in all uneven-aged conifer stands, with a 6 - 15 % increase in detection rate, and little difference in commission error (Table 2). Detection rate was considerably higher in the sparse uneven-aged stand than the dense stands, simply because trees in the former were more isolated, which facilitated detection by both algorithms. Commission error was noticeably higher in two uneven-aged conifer stands (Table 2, stands PEF-15 and PEF-28), possibly due to their field inventories having been conducted five years prior to the first LiDAR acquisition. Within those five years small trees may have grown to 11.4 cm or greater, allowing their detection with LiDAR and not with field data. We believe many of the commission errors noted for all stands and both algorithms can be attributed to the detection of small trees (< 11.4 cm DBH).

Watershed delineation yielded a slightly higher detection rate in the dense even aged conifer stands, detecting 6% more trees, though at the cost of considerably more commission errors (Table 2). These stands were of a sufficient canopy density to block LiDAR returns from all but the upper most canopy. As a consequence, layer stacking was less likely to detect areas of high overlap density throughout the lower canopy strata.

Both layer stacking and watershed delineation performed equally in the pre-commercially thinned conifer stand (Table 2, AP site), which most closely resembled plantation-like conditions. Point cloud density was 6 pls/m² in this stand in contrast to the 21 pls/m² used in the PEF. Despite this limitation, the detection rate was relatively high (74%) for both algorithms, likely owing to the structural homogeneity and wider spacing of the stand. Trees with greater horizontal spacing tended to be more easily delineated by both algorithms.

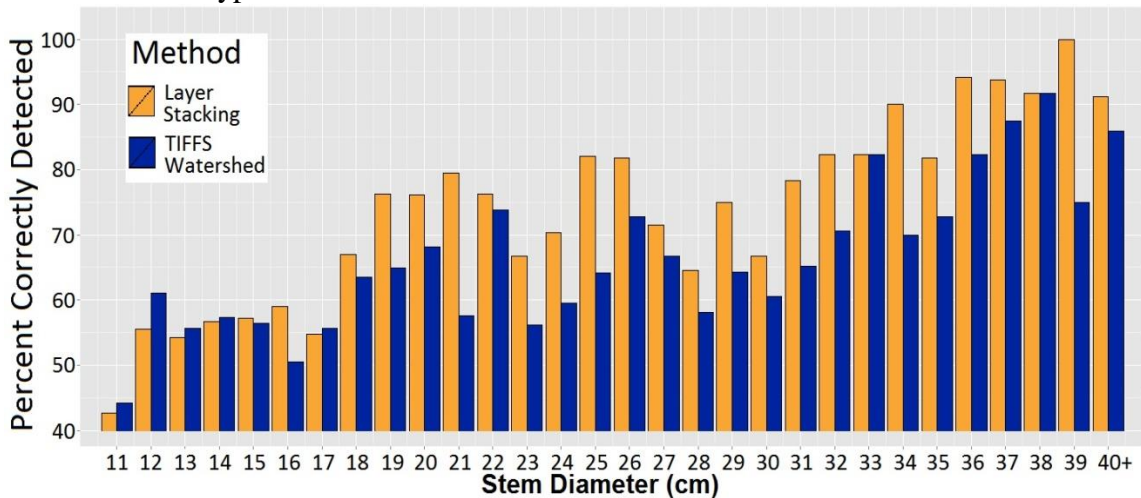
Both algorithms performed less well in the dense mixedwood stand (Table 2, NRF). This stand had a highly complex vertical canopy structure, without distinct stratification, as well as a diverse, spatially integrated mix of tree species. There were numerous instances of *Acer rubrum* clumping (stems arising from stump sprouts), making both detection and segmentation difficult. Despite this difficulty, layer stacking had a 10% higher detection rate than watershed delineation, with a 2% increase in commission error. Point density was also lower in the dense mixedwood stand (NRF site), at only 5 pls/m². This limitation may have contributed to the low detection rates of both watershed delineation and layer stacking (43 and 53% respectively, Table 2). When segmenting trees with a complex or uneven age structure, more LiDAR returns will likely yield better results, regardless of the algorithm employed.

The most notable difference in algorithm performance can be seen in the pure deciduous stand, at least in the leaf-off conditions tested here. Layer stacking had a detection rate 29% higher than that of watershed delineation, with nearly equal commission error. As noted above, watershed delineation may not perform well in deciduous forests with dense interlocking crowns because of a lack of distinct peaks and troughs. Layer stacking on the other hand, appears to perform better under these conditions because of increased laser penetration to the center of the tree. The performance of layer stacking seems to improve when laser returns off the tree bole can be observed at each 1-m layer.

Detection rates also varied by individual tree size. Figure 1.4 displays detection rates of both layer stacking and watershed delineation across each 1-cm diameter class for all trees measured. Layer stacking and watershed delineation's ability to detect small

trees (generally less than 18 cm DBH) was nearly equal. Trees with diameters of 18 cm or greater were more likely to be detected by layer stacking than by watershed delineation. An exception to this trend occurred in the pure deciduous stands, in which layer stacking's detection rate was consistently higher across all diameter classes. In these stands, layer stacking detected 32% more trees than did watershed delineation with diameters less than 18 cm, and 28% more trees with diameters greater than 18 cm.

Figure 1.4: Detection rate displayed by stem diameter. Detection rates for both layer stacking and Toolbox for LiDAR data Filtering and Forest Studies (TIFFS) watershed algorithm are shown below by 1-cm diameter class (DBH rounded to the nearest cm) across all forest types.



Discussion

Layer stacking shows promise as a novel method for segmentation, with improved detection rates over traditional watershed delineation in every stand type and composition we evaluated, except the dense even-aged conifers. However, layer stacking has several shortcomings worth noting, which could likely be improved by additional refinements.

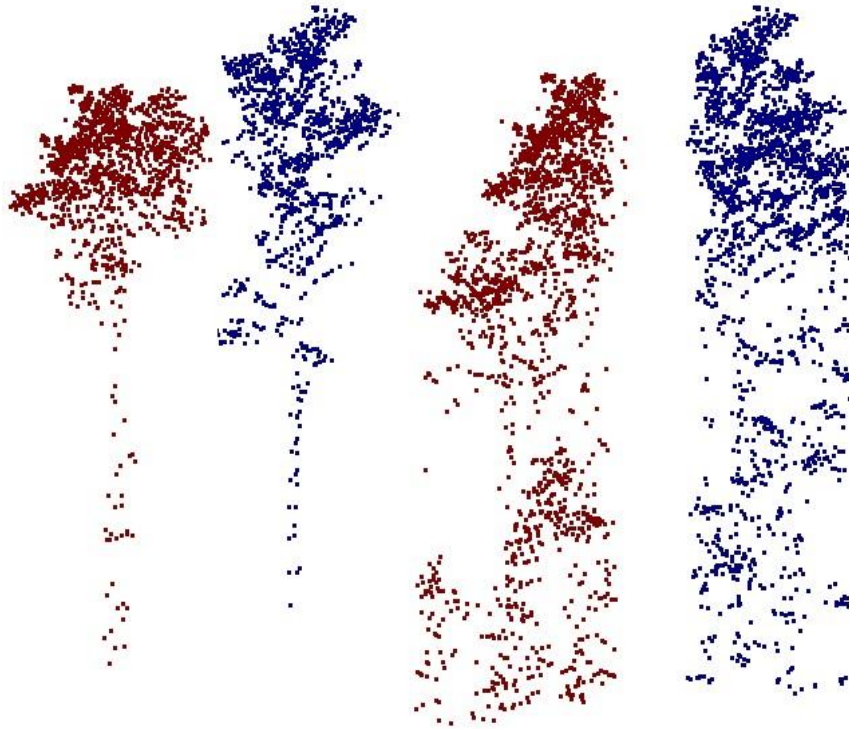
First, conifers often only yield returns on the surface of their crowns, leaving a hollow interior. Ideally the clustering algorithm used in layer stacking corrects for this by grouping all peripheral crown points together, and then filling in the center. In practice,

however, emergent conifers (mostly *Pinus strobus* in the region tested) could be inadvertently broken into smaller pieces, as the crown perimeters provided more overlaps than do the tree centers. A similar problem occurs in deciduous trees in leaf-on conditions, as fewer laser pulses encounter the tree bole, making detection more difficult. One potential solution is to fly LiDAR with a high scan angle, allowing for more side penetration into the crown, as was done with all LiDAR here. Another solution is to simply fly higher density LiDAR, as more pulse returns would increase the chance of detecting the tree bole.

Second, increases in detection rate must be weighed against the computational inefficiency of layer stacking when compared to watershed delineation. Though computation time and overall efficiency were not recorded, nor were they included in our objectives, we note that layer stacking's computation time increases exponentially with plot size or point cloud density. The greatest inefficiency stems from the hierarchical clustering technique used, which calculates a complete point-point distance matrix for each horizontal layer in the forest. Thus, for small plots, clustering was nearly instantaneous; however, as segmentation area increased to multiple hectares, computation time of the clustering algorithm slowed considerably. We believe that there are several improvements that can be made to the clustering algorithm's implementation. A more automated clustering algorithm that required no user validation and was capable of adapting to forest type, LiDAR density, and layer level would be a considerable improvement to the algorithm's efficiency and effectiveness. These improvements are currently being explored.

Third, in terms of characterizing crown shape, both layer stacking and watershed delineation have room for improvement. Because watershed delineation often mistakenly included smaller trees within or around the crowns of primary trees, we feel it tended to overestimate crown size. On the other hand, layer stacking often excluded layers that were farthest from the tree center, which tended to underestimate crown size. The extensive error filtering conducted on each layer had the effect of removing abnormally large clusters, most of which represented the outer portions of the tree crown. When calibrating the error filters for layer stacking, the choice had to be made between full tree crowns, which may have included some erroneous layers of neighboring trees, or narrow crowns, which may have excluded some valid layers. Figure 2c illustrates this tradeoff. In the latter case, while the outside canopy envelop may have been slightly clipped, we feel that the shape of the extracted tree's skeletal structure is improved considerably. While watershed delineation extracts every point beneath a blanketed area covered by the tree's canopy, layer stacking selects portions of the tree at each level. Thus, trees were more reliably extracted beneath the surface of the canopy. Beneath the live crown, it is not uncommon for layer stacking to extract only the tree bole, and watershed delineation to extract all low lying vegetation surrounding the tree (Fig. 1.5). The extraction of the bole may prove useful in further analysis of the tree, such as stem diameter measurements (Bucksch et al. 2014) or stem form estimates.

Figure 1.5: Comparison of results between layer stacking and watershed delineation. The two trees on the left were segmented via layer stacking; same two trees on the right were segmented via watershed delineation. Layer stacking produced a point cloud that better represents the bole and lower portion of the tree, while watershed delineation segmented every point below the surface, including extraneous features not belonging to the tree.



Though tree crown position (dominant, co-dominant, intermediate, overtopped) was not measured in the field, inferences can be made by examining detection rate of each algorithm by diameter class (Figure 4). As small-diameter trees are more frequently overtopped in most of the uneven aged stands, it can be inferred that layer stacking's noted improvements in detection rate in most stands was due to enhanced detection of intermediate, co-dominant, and dominant trees. Watershed delineation may have had difficulty segmenting co-dominant and intermediate trees, which blended in to the watershed profile of larger adjacent trees. An exception to this occurred in deciduous stands, where layer stacking detected more trees in every diameter class. This finding

may indicate that layer stacking was better able to detect overtopped trees in these stands. Qualitatively, this appeared to be the case. This could be explained by the greater penetration noted in leaf-off deciduous trees, making the overtopped trees below them visible, and because the canopy above did not block the overtopped tree's signal on the overlap map as it would on a CHM.

Thus, we feel that improvement could also be made to the segmentation of overtopped trees. As it stands, detection rate of overtopped trees from the overlap map appears qualitatively high. However, many of those trees were erroneously segmented or filtered out in subsequent steps, and as such, the reported detection rates suffered. In the event that a small tree is detected on the overlap map (signified by few overlaps), it might be beneficial to subject it to further scrutiny, perhaps including only clusters beneath a certain height threshold, or attempting to identify gaps in the vertical strata representing the space between the overtopped and dominant tree, similarly to the method used by Duncanson et al. (2014) with watershed delineation.

Conclusions

We developed and tested the layer-stacking algorithm in what we consider to be very challenging forest conditions, namely mixedwood stands with vertically complex crown structures, including numerous overtopped trees. Despite the areas for improvement discussed above, we believe that layer stacking, when applied to these forest types, provides a reasonable alternative to watershed delineation, currently the most commonly used segmentation algorithm. Improvements were noted in both detection rate and crown shape. Layer stacking appears to be particularly well suited for deciduous leaf-off data sets. We believe layer stacking contributes to the rapidly growing

advancements in individual-tree based approaches in the use of aerial LiDAR data, all hopefully leading to the increased accuracy and efficiency of forest inventories.

CHAPTER TWO:
DETERMINATION OF INDIVIDUAL TREE SPECIES, DIAMETER, VOLUME,
AND CARBON STOCK FROM AIRBORNE LIDAR FOR LARGE-SCALE
STAND INVENTORIES IN MIXED SPECIES FORESTS

Introduction

In the last two decades airborne light detection and ranging (LiDAR) has proven an invaluable asset for forest inventories (White et al. 2013). LiDAR creates a three-dimensional point cloud representing forest canopy structure, and interpretation of that point cloud can yield information on forest attributes such as tree basal area, tree stem volume, and forest carbon stocks. As the technology's capabilities have increased, so too has the demand for more precise estimates. Such estimates could be of great value to modern foresters, aiding in issues that require a high degree of precision, such as managing complex stands or assessing carbon stocks.

There are currently two primary means of obtaining forest biometric data from LiDAR point clouds. First, and most common, is the area-based (AB) approach, which makes use of LiDAR point metrics such as height percentiles, maximum height, and mean height of points within a plot. By combining these metrics with field measurements from the same stands, statistical models can be developed that predict desired attributes in other locations within a similar forest type (Næsset 2002). Many studies have shown that plot-level basal area, height (Means et al. 2000), biomass (Zolkos et al. 2013), volume (Naesset 1997), and tree density (Næsset and Bjercknes 2001) can be accurately predicted using AB methods. These methods, however, are limited to generalized

estimates of plot or stand stand-level attributes, and yield no information about the individual trees within each plot.

The second method is the individual-tree-crown (ITC) approach, which segments a LiDAR point cloud into areas representing individual trees, and then retrieves metrics from each tree separately, often summing them to achieve plot or stand level estimates (Hyypä and Inkinen 1999). It is not uncommon to combine this approach with the AB approach, using AB estimates to correct erroneous ITC estimates (Maltamo et al. 2004, Lindberg et al. 2010, Breidenbach et al. 2010). Since the ITC approach provides detailed information on each tree, it has several benefits over AB approaches: each tree's coordinates and attributes are made available to forest managers, tree species is easier to estimate (Vastaranta et al 2009), considerably less field work is required for estimates, and the methods behind ITC inventories often bear a greater resemblance to field based inventories, making them more intuitive to forest managers (Breidenbach and Astrup 2014).

Despite these benefits, the ITC approach is rarely used operationally due to the difficulty in segmenting trees from a LiDAR point cloud. Accuracy of plot and stand level estimates derived from the ITC approach are highly correlated with individual tree detection rates. In a comparison between ITC and AB approaches with low resolution LiDAR, Vastaranta et al. (2009) showed that on a plot level, ITC basal area and volume estimates were less reliable than AB estimates, with the former consistently producing underestimates presumably due to undetected trees, but that tree height and diameter estimates were more reliable. Similarly, Yu et al. (2010) and Vastaranta et al. (2011) reported little difference between the two methods, while Peuhkurinen et al. (2007)

achieved superior results with the ITC approach. Each study noted, however, that accuracy could be improved with better segmentation methods. There is therefore disagreement over which method yields better results, with the general consensus being that as LiDAR pulse density and segmentation methods improve, the increased information provided by the ITC approach can be of benefit for forest analytics.

As a consequence, much effort has been devoted to developing algorithms for individual tree segmentation. Current segmentation algorithms include watershed delineation (Chen et al. 2006), local maxima detection (Persson et al. 2002), and clustering (Morsdorf et al. 2003). Individual tree detection rates depend highly upon forest type and segmentation method used (Kaartinen et al. 2012). In a comparison of several segmentation methods, Vauhkonen et al. (2011) reported tree detection rates ranging between 40 and 80%. Many other studies have detection rates that fall within this range, though detection rates in deciduous forests have traditionally been considerably lower than coniferous ones (Koch et al. 2006, Brandtberg et al. 2003). In this paper, we use a newly developed segmentation method known as *layer stacking*, which yields higher detection rates across most of the forest stand types to which it was applied, when compared to the popular watershed delineation algorithm (Chapter 1). Layer stacking produced overall detection rates between 55% and 85%, depending on forest stand type. Leaf-off deciduous stands consistently had the highest detection rate due to increased laser penetration of the canopy, while uneven aged coniferous stands had the lowest detection rate for the opposite reason.

As mentioned above, ITC has the additional benefit of potentially identifying the species of each segmented tree, which allows for more accurate tree attribute estimates

derived from species-specific allometric equations. Previous studies have explored species classification from LiDAR using laser return intensity (an analog for infrared reflectance), full waveform information, and structural characteristics (Brandtberg 2007, Kim et al. 2009, Korpela et al. 2010, Li et al. 2013). Other studies have paired LiDAR data with multispectral or hyperspectral imagery to aid in species classification and segmentation (Asner et al. 2008, Naidoo et al. 2012, Ørka et al. 2012). In this study, we identify tree species by comparing intensity values between summer and winter LiDAR data sets, combined with analyses of structural and shape characteristics of each tree.

The objective of our study was to test a sequence of methods for obtaining accurate ITC estimates of species, stem diameter, stem volume, and ultimately carbon stock for each tree in the forest. Briefly, once trees were segmented and identified to species, canopy structure metrics obtained from the point clouds were used to estimate tree diameters. These were used, in combination with height measurements, to estimate stem volume and ultimately above-ground biomass for each tree, via species-specific allometric equations. Validation of our estimates (stem diameter, stem volume, and carbon content) was done at the tree, plot, and stand level. Tree and plot estimates were validated against field measurements, while plot and stand estimates were validated against AB estimates. This approach represents a complete bottom-up analysis, with comparison of biometrics at each level traditionally useful to forest managers.

Throughout the process we came to several conclusions: we validated the effectiveness of the layer stacking algorithm for generating proper crown metrics; we evaluated the effectiveness of species-level predictions, concluding that it is possible to accurately make the distinction between coniferous and deciduous species, and possible to predict

conifer species with reasonable accuracy; and we illustrated that the ITC approach as presented here can predict volume as well or better than a common AB approach, and predict stem diameter and carbon stock with a reasonable degree of accuracy.

Methods

Study Area

To assess the validity of the biomass estimates, a site was needed that had a variety of forest stands structures and compositions, as well as field-measured data which included spatial coordinates, heights, diameter at breast height (DBH, 1.37 m), canopy widths, and species of many individual trees. The site we selected was the University of Maine Foundation's Penobscot Experimental Forest, which had a wide range in silvicultural treatments and field data on thousands of trees.

Plots used for verification were fixed-area plots of either 16 or 20 m radius. The centers of all plots were taken via consumer grade GPS; those plots used for ITC validation were shifted *a posteriori* so that the individually mapped trees aligned with the LiDAR data, since a greater degree of spatial accuracy was needed. All trees greater than 11.4 cm DBH had species, height, and DBH measured. A total of 205 plots were used for the AB model calibration, while a different set of 22 plots were used for validation.

LiDAR

Two LiDAR datasets were collected. The first LiDAR acquisition took place in June, 2012, with NASA Goddard's LiDAR, Hyperspectral, and Thermal Imager (Cook et al. 2013) at an average of 15 ppm, with a pulse rate of 300 Khz, an average footprint size of 10 cm, a 28.5 degree maximum scan angle from nadir, and an altitude of

approximately 335 m above ground level (NASA data). The second LiDAR dataset was acquired in October, 2013, in leaf-off conditions with a RIEGL LMS-Q680i at an average of 6 ppm, with a pulse rate of 150 Khz, an average footprint size of 0.17 m, a 28.5 degree maximum scan angle, and at an altitude of approximately 600 m above ground level (LEGEO data). The two datasets were combined visually by aligning easily identified objects. This alignment appeared valid throughout the entire dataset, and trees were not shadowed nor distorted. Thus the final average point density was ~ 21 ppm. Ground points were classified by the providers. Both datasets were collected at a 1550 nm wavelength. This combination was beneficial because it provided more structural information for the layer stacking algorithm and aided in species identification due to seasonal differences in intensity. All measurements are assumed to be from the latter acquisition date.

Individual Tree Segmentation

Individual tree segmentation was done *via* layer stacking (Chapter 1), as shown in Figure 1.1 and 1.2. Briefly, the algorithm proceeds by splitting the LiDAR point cloud into horizontal layers at 1 m intervals (Fig. 1.1a), then applying clustering algorithms to each layer to identify clumped points representing trees (Fig. 1.1b). The lowest three meters are subject to density based scanning (Ester et al. 1996) while the rest are subject to hierarchical agglomerative clustering (Müllner 2013). Polygons are placed around each cluster of points at each layer (Fig. 1.1c), and the polygons are then stacked on top of one another. A map of the number of overlapping polygons throughout the canopy strata is the created, similarly to a Venn-diagram (Fig. 1.1d). The overlap map is smoothed (Fig. 1.1e), and local maxima are detected, and presumed to represent the centers of trees (Fig.

1.1f). All polygons then touching these tree centers are then assumed to be a part of that tree's crown (Fig. 1.2a). Erroneous polygons are then removed through a series of error filtering (Fig. 1.2c). Each polygon is then extruded into three-dimensional space at its appropriate layer, forming the three-dimensional shape of the tree (Fig. 1.2b). Finally, all LiDAR points lying within this shape are clipped into separate point clouds and assigned a unique identifier.

Individual Tree Measurements

We tested the utility of 28 attributes of individual tree point clouds (see Table 2.1) for predicting tree species and stem diameter. Attributes such as intensity and reflectance for each LiDAR dataset were measured for every point within each segmented tree. These constituted a measure of infrared albedo of the tree at a 1550 nm wavelength which is determined by leaf size, orientation, density, and reflectance (Korpela et al. 2010). The calculations behind these number differed by LiDAR provider; thus, this measure is referred to as 'reflectance' for the NASA dataset, and 'intensity' for the LEGEO dataset. In addition, crown width and density histograms were constructed for each tree by dividing the segmented tree into 1-m height intervals and measuring maximum crown width and point count at each interval. These histograms were then analyzed by measuring skewness, kurtosis, and the mean first-order difference, the latter of which refers to the mean difference between successive height intervals. The location of the widest and densest level on the tree's histogram was also measured as a percent of total tree height.

Table 2.1: Tree measurements used for modeling. Variables used for the predictive models and allometric equations are listed along with a brief description.

Designation	Description
NASA_M_Int	Mean laser reflectance of each point in the tree from the NASA data.
NASA_SD_Int	The standard deviation of laser reflectance of each point in the tree from the NASA data.
NASA_90P_Int	The 90th percentile of laser reflectance of each point in the tree from the NASA data.
NASA_Int_Kurt	The kurtosis of reflectance values for each point in the tree from the NASA data.
NASA_Int_Skew	The skew of reflectance values for each point in the tree from the NASA data.
LEGEO_M_Int	Mean laser intensity of each point in the tree from the LEGEO dataset.
LEGEO_SD_Int	The standard deviation of laser intensity of each point in the tree from the LEGEO dataset.
LEGEO_90P_Int	The 90th percentile of laser intensity of each point in the tree from the LEGEO dataset.
LEGEO_Int_Kurt	The kurtosis of intensity values for each point in the tree from the LEGEO data.
LEGEO_Int_Skew	The skew of intensity values for each point in the tree from the LEGEO data.
Widest_Loc	The widest location of the tree expressed as a percentage of total height.
Densest_Loc	The densest location of the tree expressed as a percentage of total height.
Percent_Only	The percentage of single laser pulse returns in the tree.
Pointiness	A measure of crown pointiness, defined as the mean angle between the top point in the tree and the next five lowest points.
Height	The height of the highest point in the tree.
Width_Kurt	The kurtosis of a width histogram of the tree constructed from 1 m intervals
Width_Skew	The skew of a width histogram of the tree constructed from 1 m intervals.
Width_FOD	The mean of first order differences of a width histogram of the tree constructed from 1 m intervals.
Density_Kurt	The kurtosis of a density histogram of the tree constructed from 1 m intervals
Density_Skew	The skew of a density histogram of the tree constructed from 1 m intervals.
Density_FOD	The mean of first order differences of a density histogram of the tree constructed from 1 m intervals.
Ground_Ret	The density of ground returns beneath the tree's crown.
Canopy_Projection	The area of a top down convex hull of the tree's crown.
Max_Width	The largest measured width of the tree's crown from a top down view.
Corrected_Width	The diameter at which there is the largest increase in relative point count from a top down view.
Top_Density_Kurt	The kurtosis of a density histogram constructed from point count within concentric rings in a top down view of the crown.
Top_Density_Skew	The skew of a density histogram constructed from point count within concentric rings in a top down view of the crown.
Top_Density_FOD	The mean of first order differences of a density histogram constructed from point count within concentric rings in a top down view of the crown.

The pointiness of the tree's apex was quantified as the mean angle from the highest point of the tree to the next five lowest points in the tree's crown. The height of the highest point was taken to be total tree height. Two measures of laser penetrability were made for each tree: the first was the percentage of single returns, defined as percentage of laser pulses that hit the tree and returned only one signal to the sensor, as opposed to several; the second was the number of ground points per meter beneath the tree, measured by drawing a convex hull around a top-down view of the tree and measuring ground point density within that hull.

Finally, several measures of canopy width were made. The area of the convex hull was taken as canopy projection area, and the maximum width of the hull was taken as maximum canopy width. In many instances, errant portions of neighboring trees were included in the tree's crown by the segmentation algorithm, causing the maximum measures to over predict canopy size. To correct these errors, all points within the tree were projected in a two-dimensional top-down view. A center point of the tree was calculated by determining the mean of all points. From the center, ten concentric rings were drawn extending outward to the furthest most point, each with equal area. A histogram was then constructed from point counts within each of these rings, and skewness, kurtosis, and mean first-order differences were calculated. The true crown width was estimated by using the diameter of the ring with the greatest first -order difference (expressed as a percentage), with rings that had less than 5% of the total points excluded. This location represented the width at which point density sharply increased, which was taken as the outer reaches of the of the tree's actual canopy (see Figure 2).

Species Identification

Since there is a considerable amount of difference in allometry across species, each tree's LiDAR attributes were used to classify it into one of several species categories using two successive stages. The first stage separated trees as either coniferous or deciduous using logistic regression. The second stage separated the classified conifers further into four species categories representing the most prevalent trees in the study area (*Abies balsamea*, *Picea rubens*, *Pinus strobus*, and *Tsuga canadensis*) using random forest classification.

In order to construct the logistic regression predictive model for the deciduous–coniferous classification, 1,721 deciduous trees and 1,653 coniferous trees were selected from eleven forest stands. Each stand was known to be nearly purely deciduous or coniferous (>95%). A full model was created with each measurement from Table 1, and step-down regression analysis aided by the Akaike information criterion was used to determine the optimal model. The best-fitting model ultimately included the following predictive variables: NASA_Int_Skew, LEGEO_90P_Int, LEGEO_Int_Kurt, LEGEO_Int_Skew, Widest_loc, Percent_Only, Pointiness, Width_Kurt, Width_Skew, Density_Kurt, Density_Skew, Top_Density_FOD, and Ground_Ret (see Table 1 for explanation). The optimal threshold for classification (0.68) was determined as the optimal balance between sensitivity and specificity measures (Shaefer 1989).

The second stage of classification, that is, separating conifer species, was conducted using random forest regression with the randomForest package in R (Liaw and Wiener 2002). Random forest is a nonparametric modeling method that creates a series of

regression trees by splitting predictor variables. Regression trees are grown many times with subsets of the larger dataset, and then validated against other subsets. Results of each tree are weighed against one another for a prediction. The model was built using a total of 1444 training trees: 686 *Picea rubens*, 360 *Pinus strobus*, 316 *Abies balsamea*, and 82 *Tsuga canadensis*. All predictor variables listed in Table 2.1 were used in the model, as there was little risk of over fitting given the random forest technique.

Individual Tree Diameter Estimation

The best fitting model for predicting tree stem DBH from LiDAR data ultimately included the following attributes: corrected tree crown width (Corrected_width), skewness of the crown-width distribution (Width_Skew), tree height, and tree species. This model had an adjusted r-squared of 0.63 and a root mean squared error (RMSE) of 7.6 cm, or 31.6 % of the mean DBH. Diameter estimates were converted to basal areas for plot- and stand-level basal area validation, and they were used in conjunction with allometric equations to estimate volume and carbon content of individual trees.

Individual Tree Stem Volume

Estimated diameter and total height were used to calculate stem volume of each tree using regional taper equations developed by Kozak (2004) and refined by Li et al. (2012). Because these equations are species specific, weighted model averaging was used to combine the volume models of deciduous trees, which were not classified to species. Field measured relative species abundance in each stand were used to assign weights. Outer bark volume was used for all estimates where it applied.

Individual Tree Aboveground Carbon

Using the above estimated stem volume, stem biomass could be obtained using known wood densities (Harmon et al. 2008). Branch and leaf biomass was calculated using regional equations developed by Young et al. (1980) based on estimated diameter. These values were tabulated for each tree to obtain total above-ground biomass. Finally, carbon content was estimated using species specific biomass-to-carbon ratios developed by Lamtom and Savidge (2003). In the few cases where species specific ratios were not available, we used a ratio of 0.5 to estimate carbon. In the case of *Picea rubens*, the carbon ratio of *Picea glauca* was used.

Post-hoc ITC Correction

On a plot and stand level all individual tree estimates were summed within the area of interest to produce estimates on a per-hectare basis. These estimates however showed a consistent negative bias when compared to field measurements, undoubtedly due to trees missed by the segmentation algorithm. We adjusted for this bias by adding the percentage associated with omission error to each area estimate, then subtracting the percentage associated with commission error in each forest type. Because this information is often not available without field data, and thus the correction may not be practical in all circumstances, we report results without the correction (additive estimates), alongside results with the correction (corrected estimates).

Area-Based Estimation

Area-based metrics on the 205 plots used for model calibration were calculated using FUSION v3.42 (McGaughey 2009), which was developed by the U.S. Forest

Service Pacific Northwest Research Station. A total of 61 predictor variables were used, including height and intensity measurements such as percentiles, mean, median, minimums, and maximums. Random forest regression was used to estimate stem volume (m^3). Plot-level estimates were made using the whole plot, while stand-level estimates were based on 10 x 10 m blocks, with estimated volume associated with each block within the stand summed and divided by stand area. A total of 18 forest stands were used for calibration, encompassing a wide variety of forest stand types. Field measured data were collected between 2003 and 2013, making some of the measurements as much as 10 years older than the LiDAR data, the mean collection year was 2007. To account for varying sampling years, all DBH and height measurements older than the LEGEO LiDAR were projected to 2013 using the Acadian Variant of the Forest Vegetation Simulator, developed by Weiskittel et al. (2012). Overall, the methods for the AB modeling strongly resembled those used by Hayashi et al. (2014) in the same study area. Trees with diameters less than 11.4 cm were removed only after this projection. “Out-of-bag” sampling within random forest indicated that the model accounted for 85.3% of variation in the data. More in-depth analysis of model accuracy is discussed in the *Results*.

Biometric Validation

Validation was done on with 22 plots taken from seven stands, all measured within two years of the LEGEO LiDAR. Stands could be broken down into three general forest types: uneven-aged conifers, even-aged conifers, and uneven-aged deciduous. Forest attributes and silvicultural history of each stand is displayed in Table 2. All trees of sufficient size within these plots were mapped spatially in relation to plot center. Trees

were plotted in the virtual three dimensional space with the segmented LiDAR point cloud, and extruded to their field measured height. Plot centers were then shifted so as to visually align field measured trees with the LiDAR data. Field measured trees with obvious counterparts (N = 524) in the LiDAR were used for validation. Thus, each tree in the comparison had a LiDAR derived estimate and a field measured truth. Tree-level validation was done using simple linear regression, and equivalence tests were used to assess predictive accuracy. Adjusted r-squared values, RMSE, and the equivalency thresholds are reported for DBH, stem volume, and carbon content.

Table 2.2: Stand characteristics, silvicultural history, species composition, and year measured for the 11 stands under study. Stands are grouped by forest type. Stand metrics were based on trees greater than or equal to 11.4 cm DBH.

Stand Identifier	Density (trees/ha)	Basal Area (m ² /ha)	Silvicultural Treatment	Species Composition*	Year Inventoried	Number of Plots	Total Trees Measured
Uneven-aged conifers							
9	510 ± 37	29.2 ± 1.2	Single-tree selection system, 5-year cutting cycle. Last harvested 2010	35% <i>Abba</i> , 33% <i>Tsca</i> , 14% <i>Piru</i> , 9% <i>Acru</i>	2013	4	78
16	509 ± 24	25.6 ± 2.1	Single-tree selection system, 5-year cutting cycle. Last harvested 2012	39% <i>Tsca</i> , 38% <i>Abba</i> , 9% <i>Piru</i> , 7% <i>Acru</i>	2011	6	123
12	617 ± 27	28.1 ± 1.7	Single-tree selection system, 10-year cutting cycle. Last harvested 1995	52% <i>Abba</i> , 18% <i>Tsca</i> , 14% <i>Acru</i> , 9% <i>Piru</i>	2014	4	95
Even-aged conifers							
23B	1434 ± 50	30.3 ± 2.6	Uniform shelterwood, three-stage overstory removal	44% <i>Abba</i> , 31% <i>Pist</i> , 10% <i>Tsca</i> , 10% <i>Piru</i>	2011	3	159
29B	869 ± 29	17.3 ± 0.7	Uniform shelterwood, three-stage overstory removal	44% <i>Piru</i> , 25% <i>Abba</i> , 14% <i>Pist</i> , 5% <i>Bepa</i>	2011	3	76
Uneven-aged deciduous							
M1	337	21.5	Commercially thinned in 2011, reserve prior	62% <i>Acsa</i> , 7% <i>Acru</i> , 7% <i>Osvi</i> , 5% <i>Tiam</i> , 5% <i>Fram</i>	2015	1	35
M2	608	45.3	Reserve	66% <i>Acsa</i> , 9% <i>Fram</i> , 7% <i>Osvi</i> , 5% <i>Tiam</i> , 5% <i>Frgr</i>	2015	1	37

*Species abbreviations are as follows: *Abba* = *Abies balsamea*, *Acru* = *Acer rubrum*, *Acsa* = *Acer saccharum*, *Bepa* = *Betula papyrifera*, *Fram* = *Fraxinus americana*, *Frgr* = *Fraxinus grandifolia*, *Osvi* = *Ostrya virginiana*, *Piru* = *Picea Rubens*, *Pist* = *Pinus strobus*, *Tiam* = *Tilia americana*, *Tsca* = *Tsuga canadensis*

Plot-level validation was done using the same 22 plots. Each LiDAR segmented tree whose center point lay within the plot radius was tallied. Each field measured tree was also tallied, whether identified in the LiDAR segmentation or not. Basal area (m^2/ha), stem volume (m^3/ha), and carbon mass (kg/ha) were calculated for each plot. Simple regression was once again used to assess accuracy, with adjusted r-squared and RMSE reported for both the additive and corrected plot level estimates. Adjusted r-squared and RMSE in comparison to the field model were also reported for the AB volume estimates.

Finally, stand-level comparisons were made between the corrected ITC approach, and the AB volume estimates for 8 stands; five from the uneven-aged conifer type, two from the even-aged conifer type, and one from the uneven-aged deciduous type. Field measured basal area (averaged from several plots within each stand) ranged from 7.5 to 33.4 m^2/ha . Field measured trees per ha ranged between 319 and 1434. Volume estimates from all 10 x 10m blocks within each stand were tallied and compared to the summed volume of all segmented trees within that stand, along with the post-hoc error correction. As above, adjusted r-squared, RMSE, and bias is reported in the results. No field data were available at this level.

Results

Segmentation

Segmentation detection rates varied by forest stand type (Table 2.3). Mean detection rate (defined as the percent of trees accurately detected) in uneven-aged conifer stands was 61%, with 17% commission error. Mean detection rate in dense even-aged

conifer stands was 65%, with 26% commission error. Detection was highest in deciduous stands, with a mean detection of 80% and a mean commission error of 23%.

Table 2.3: Detection rate results by stand and forest type. Total number of trees are displayed, alongside number of trees correctly detected, detection rate, and commission error. Number of trees used for the tree level validation is also displayed.

Stand Identifier	Total Trees Measured	Number of Trees Correctly Segmented	Detection Rate	Commission Error	Number of Trees Used for Validation
Uneven-aged conifers					
PEF-9	164	90	55%	11%	78
PEF-16	256	157	61%	15%	123
PEF-12	210	131	62%	12%	95
Total	630	378	60%	13%	296
Even-aged conifers					
PEF-23B	343	220	64%	18%	159
PEF-29B	211	139	66%	34%	76
Total	554	359	65%	24%	235
Uneven-aged deciduous					
PEF-M1	61	52	85%	36%	35
PEF-M2	76	54	71%	10%	37
Total	137	106	77%	28%	72

Species Identification

The first model, deciduous vs. coniferous classification, was assessed by measuring classification accuracy of 1000 deciduous and 1000 coniferous trees withheld prior to model building. In total 97.8 % of deciduous trees were correctly identified as such, while 97.5 % of coniferous trees were correctly classified, for an overall classification accuracy of 97.7%. We note, however, that classification of coniferous trees in stands that were primarily deciduous, and deciduous trees in stands that were

primarily coniferous had lower classification accuracy. Table 4a displays detection rate and commission error of the model.

The second model, classifying coniferous species, was assessed using out-of-bag error estimation within the random forest model, which uses the bootstrapped data subsets to assess accuracy of each of the component models. Table 4b shows a confusion matrix displaying accuracy of each species' classification, along with commission and omission error. *Tsuga canadensis* had the lowest accuracy with 63% correct classification, likely due to the low number of training trees used. *Picea rubens* and *Abies balsamea* were most frequently confused with one another, with 9% *Picea rubens* mistaken for *Abies balsamea*, and 18% of *Abies balsamea* mistaken for *Picea rubens*. This misclassification is likely due to similarities in crown shape. *Pinus strobus* was most frequently confused with *Picea rubens*, with 13% mistakenly classified as such. Overall classification accuracy of conifer species was 83%.

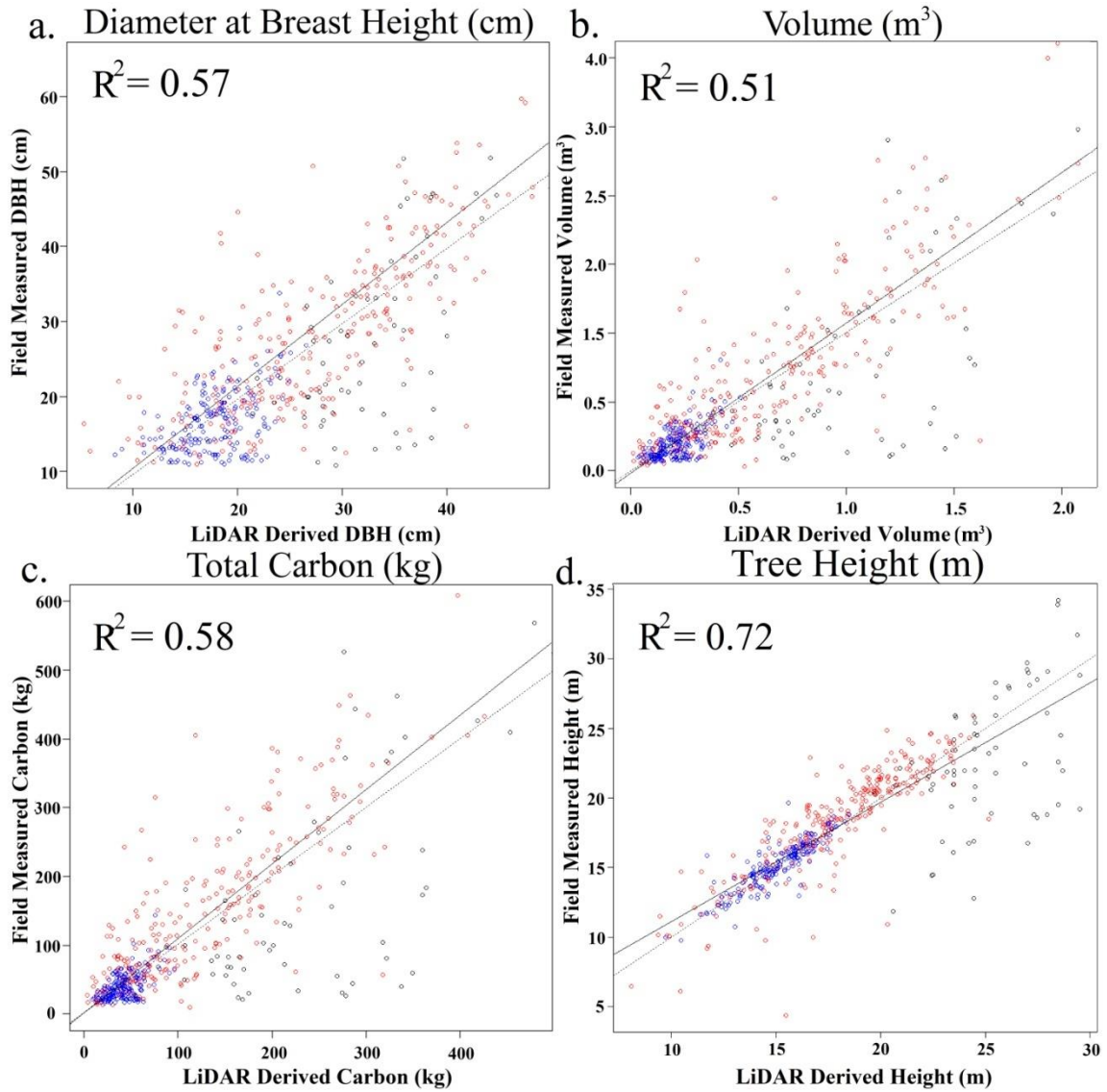
Table 2.4: Species classification confusion matrix. The matrix shows out-of-bag accuracy and classification error for the coniferous species classified by the random forest model.

Species	<i>Picea rubens</i>	<i>Abies balsamea</i>	<i>Tsuga canadensis</i>	<i>Pinus strobus</i>	Accuracy
<i>Picea rubens</i> (n = 686)	604	59	5	18	88%
<i>Abies balsamea</i> (n = 316)	58	240	9	9	76%
<i>Tsuga canadensis</i> (n = 82)	6	19	56	1	68%
<i>Pinus strobus</i> (n = 360)	45	10	3	302	84%

Tree Level Validation

Stem diameter estimates from the predictive diameter model were compared to those taken in the field for each identified tree in the LiDAR (Fig. 2.1a). Simple linear regression yielded an adjusted r-squared of 0.57. The model had a RMSE of 7.1 cm, or 29% of mean. An equivalence test indicated significance ($\alpha > 0.05$) between the field measurements and estimates at a confidence interval of 1.1 cm, or 5% of mean.

Figure 2.1: Tree level comparisons between field measurements and LiDAR estimates. Field measurements of stem diameter at breast height (DBH), stem volume, total aboveground carbon, and tree height are compared to LiDAR derived estimates. The light grey line shows the 1:1 line, the solid is best fit. Blue dots represent trees from the dense even-aged coniferous stands, red dots from the dense uneven-aged coniferous stands, and black from the deciduous stands.



Stem volume estimates incorporated both height and diameter, and as a consequence were slightly more prone to error. Figure 2.1b and d shows the simple linear regression comparing LiDAR-derived estimates and field measurements for both volume

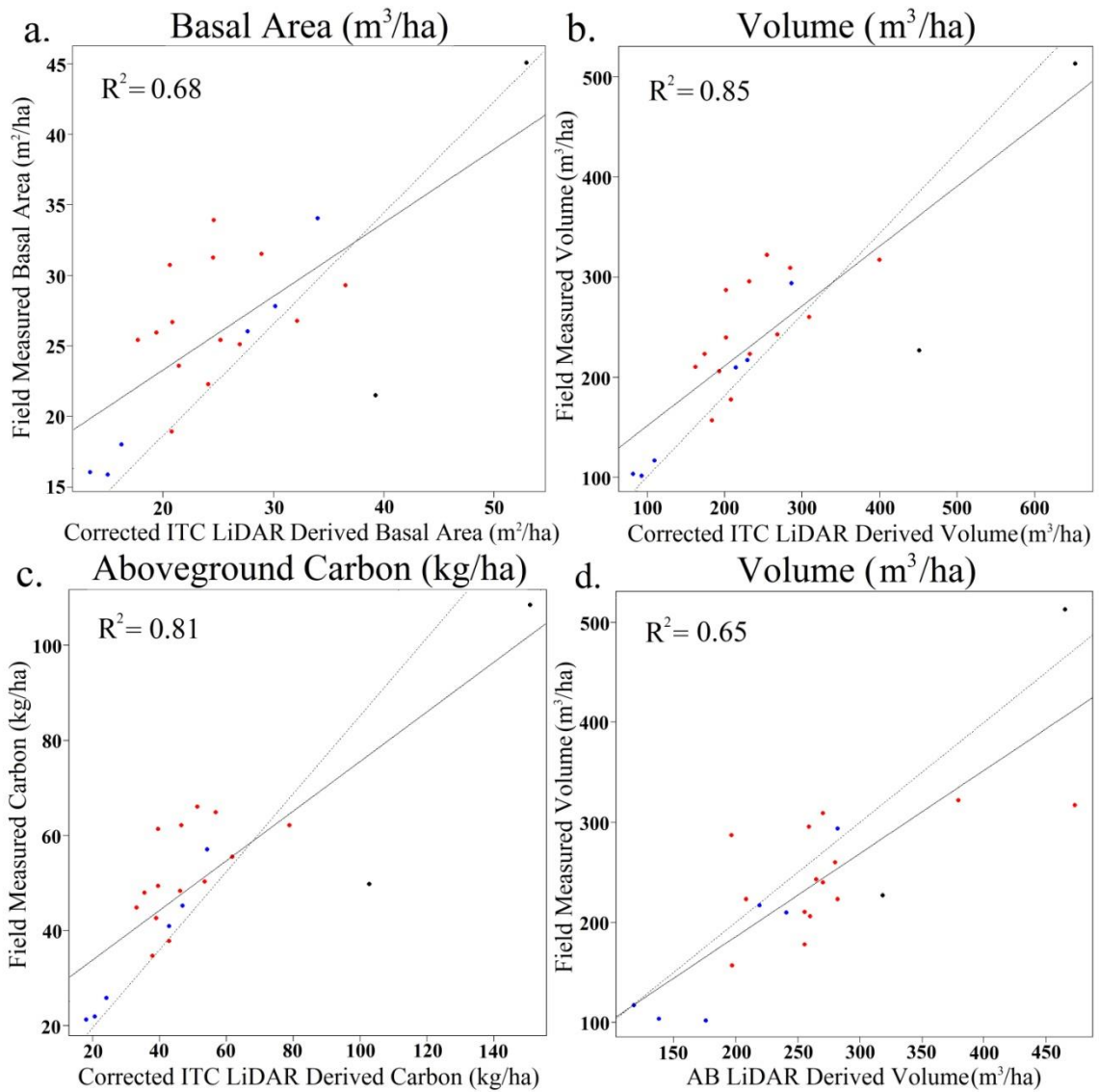
and height respectively. The volume model had an adjusted r-squared of 0.51, and a RMSE of 0.48 m³, or 87% of mean. An equivalence test indicated significant equivalence at a confidence interval of 0.09 m³, or 16% of mean.

Finally, results of the aboveground carbon estimation are shown in Figure 2.1c. The comparative model had an adjusted r-squared of 0.58, and a RMSE of 85 kg of carbon, or 74% of mean. An equivalence test indicated significant equivalence at a confidence interval of 19 kg, or 16% of mean.

Plot Level Validation

As with individual tree validation, simple linear regression was used to compare LiDAR-derived estimates with field measurements. A regression between additive ITC LiDAR estimates and field measured basal area per ha and yielded an adjusted r-squared of 0.48, and a RMSE of 4.61 m²/ha, or 17% of mean. The additive method resulted in a mean negative bias across all plots of -11.4%. Corrected plot-level estimates had an adjusted r-squared value of 0.68 (Fig. 2.2a), and a RMSE of 3.62 m²/ha, or 14% of mean. Corrected plot-level estimates had a mean positive bias of 5% across all plots.

Figure 2.2: Plot level comparisons between field measurements, layer stacking, and area-based estimates. (a-c) Field measured basal area, stem volume, and carbon content are compared to corrected individual tree crown (ITC) LiDAR estimates in each plot. (d) Field measured stem volume is compared to area based (AB) LiDAR estimates in each plot. The light grey line shows the 1:1 line, the solid is best fit. Blue dots represent trees from the dense even-aged coniferous stands, red dots from the dense uneven-aged coniferous stands, and black from the deciduous stands.



Simple regression between the additive LiDAR ITC estimate and the field measured plot estimates of stem volume and had an adjusted r-squared of 0.69, and a RMSE of 47.4 m³/ha, or 20% of mean. The additive ITC volume estimates had a negative mean bias of 8.2% across all plots. Regression between corrected ITC volume estimates

and the field measures produced an r-squared of 0.85 (Fig 2.2b), and a RMSE of 34.2 m³/ha, or 14% of mean. The corrected estimates had a positive mean bias of 8%. Plot level AB volume estimates were also compared to field data using simple regression. The adjusted r-squared of the model was 0.65, which was somewhat lower than the out-of-bag estimate (Fig 2.2d). The RMSE of the AB estimates was 50.75 m³/ha, or 21% of mean, with a positive mean bias of 14.6% across all plots. Table 2.5 shows the totals and biases for each of the three volume estimate approaches, alongside field measurements.

Table 2.5. Plot level volume estimates and biases. Field measured volume (m³/ha) are reported for each plot used in the validation alongside the uncorrected additive individual tree crown (ITC) LiDAR estimates, the corrected ITC LiDAR estimates, and the area based LiDAR estimates and their respective biases.

Stand Identifier	Plot Number	Field Measured Volume (m ³ /ha)	Additive ITC Estimate (m ³ /ha)	Percent Bias From Field	Corrected ITC Estimate (m ³ /ha)	Percent Bias From Field	Area Based Estimate	Percent Bias From Field
Uneven-aged Conifer								
PEF-9	14	318.0	343.8	+8%	460.1	+45%	473.6	+49%
PEF-9	21	322.6	225.8	-30%	302.5	-6%	379.5	+18%
PEF-9	23	223.7	160.9	-28%	215.6	-4%	208.2	-7%
PEF-9	32	240.2	183.4	-24%	245.8	+2%	270.5	+13%
PEF-16	11	223.5	208.4	-6%	256.3	+15%	282.3	+26%
PEF-16	12	206.5	176.3	-15%	216.8	+5%	260.1	+26%
PEF-16	22	243.4	243.4	-3%	291.6	+20%	264.8	+9%
PEF-16	31	178.1	178.4	+6%	231.6	+30%	255.4	+43%
PEF-16	34	157.4	157.4	+7%	207.4	+32%	196.8	+25%
PEF-16	56	296.1	296.1	-30%	254.9	-14%	258.8	-13%
PEF-12	12	309.5	250.4	-19%	315.4	+2%	240.9	-22%
PEF-12	15	260.7	269.9	+4%	340.1	+30%	270.2	+4%
PEF-12	32	211.0	151.0	-28%	190.3	-10%	280.2	+33%
PEF-12	43	287.4	183.4	-36%	231.1	-20%	255.4	-14%
Even-aged Conifer								
PEF-23B	13	210.2	193.1	-8%	227.8	+8%	196.7	-6%
PEF-23B	22	294.7	251.4	-15%	296.7	+1%	282.2	-4%
PEF-23B	31	217.7	205.6	-6%	242.7	+11%	219.0	+1%
PEF-29B	11	117.4	108.1	-8%	108.1	-8%	117.8	0%
PEF-29B	23	104.1	86.0	-17%	86.0	-17%	138.1	+33%
PEF-29B	35	102.1	94.6	-7%	94.6	-7%	175.8	+72%
Uneven-aged Deciduous								
PEF-M1	1	227.5	385.0	+69%	304.1	+34%	318.6	+40%
PEF-M2	1	513.9	548.6	+7%	652.8	+27%	465.8	-9%

The comparison between additive ITC estimation of carbon stocks and field measurements produced an adjusted r-squared of 0.66 (Fig. 2.2c), with a RMSE of 10.3 kg/ha of carbon, or 21% of mean. The additive ITC estimates had a negative bias of 10.3%. The corrected ITC estimates had an adjusted r-squared of 0.81, and a RMSE of 7.61 kg/ha, 15% of mean. The corrected ITC estimates had a positive bias of 5.2%.

Stand Level Validation

At a stand level corrected ITC volume estimates were compared to AB volume estimates. Simple regression yielded an adjusted r-squared of 0.98, and a RMSE of 106 m³, or 6% of mean. On average the AB estimates were 5% greater than the corrected ITC volume estimates.

Discussion

Segmentation accuracy of layer stacking was extensively tested in the study area and compared to a commercial watershed delineation algorithm in Chapter 1. The layer stacking algorithm performed exceptionally well in the deciduous stands, which is unusual for most ITC algorithms. Though there was room for improvement in terms of detection rate in both conifer stands, this must be weighed against the structural complexity of the uneven-aged conifer stands, and the very high density of the even-aged conifer stands.

Results of the species classification from LiDAR point clouds showed promise, particularly in the separation of coniferous and deciduous species. This classification yielded a high accuracy with the withheld data. This result was somewhat expected, as the difference between the two groups was apparent visually in both LiDAR datasets

when viewing by intensity or reflectance. This figure was slightly higher the 90.6% deciduous vs. coniferous accuracy reported by Kim et al. (2009) using similar methods with two datasets from different seasons, and on par with the 96% reported by Reitberger et al. (2008) who used leaf off LiDAR and analyzed waveform characteristics. We believe that the intensity measurements, the percent of single returns, the ground point density, and the tree's pointiness were the most important predictor variables (mostly based on p-value); the latter two have not traditionally been used in ITC analyses. Qualitatively, the classification appeared slightly less accurate when classifying trees embedded in the opposite stand type. One explanation for this could be that the deciduous trees used for training were all mature and shade tolerant species, while those normally found interspersed in a conifer stand would likely be smaller and shade intolerant species, having slightly different canopy characteristics.

The conifer species classification showed a reasonable ability to separate the conifer species, with an overall accuracy of 83%. Classification of *Tsuga canadensis* had the lowest accuracy, likely because of the lack of training trees available for model calibration. In contrast, *Picea rubens* and *Pinus strobus* had the highest accuracy, likely because of the relatively large number of training trees available. *Picea rubens* and *Abies balsamea* were most frequently confused with one another, likely owing to their similar canopy shapes. *Abies balsamea*, is often more pointed however, and tended to be smaller on the study site. Relative importance of the various predictors was estimated for the random forest model, revealing that height, intensity variables, percent only, and ground point density were the most important predictors. It was noted upon examination of intensity/reflectance from both LiDAR datasets that conifer species as well as different

deciduous species could be visually distinguished from one another, although this differed somewhat between the two datasets. For example, *Picea rubens* was consistently darker than other conifers in the NASA dataset, while not being noticeably different in the LEGEO dataset. This could be caused by the aforementioned differences in the intensity/reflectance calculations or by seasonality. No studies have been conducted classifying the conifer species in the region of study, however, many studies have classified conifer species with approximately the same success. In Ontario, Li et al. (2013) achieved a 77% classification accuracy between the species *Pinus strobus*, *Pinus banksiana*, *Acer saccharum*, and *Populus tremuloides*. In Montana, Suratno et al. (2009) achieved accuracies between 65-95% accuracy depending on crown class between the species *Pseudotsuga menziesii*, *Larix occidentalis*, *Pinus ponderosa*, and *Pinus contorta*. While in Finland, Vauhkonen (2010) achieved an accuracy of 78% classifying *Pinus sylvestris*, *Picea abies*, and deciduous trees.

Results of the tree-level analysis indicated a moderate degree of variability in all three LiDAR-derived estimates (diameter, volume, and carbon) when compared to the field data. Given that most existing allometric equations rely on accurate DBH measurements, this is arguably the most critical attribute we have estimated. There are several ways of estimating DBH from an individual tree's point cloud. One approach is to model the desired attribute directly, often using height metrics similar to the AB approach, effectively treating each tree like a small plot (Villikka et al. 2007, Yu et al. 2011). The alternative is to use only 'direct' measurements, and use existing allometric equations to then estimate the desired attribute (Vastaranta et al. 2011), a method preferred in some cases for its similarity to field inventories and lack of required field

work. In this study we choose to model stem diameter from a measure of canopy width, estimated species, and tree height, all of which have well known strong correlations to stem diameter in the region studied (Russell and Weiskittel 2011, Rijal et al. 2012). We attempted to mirror field based inventories by using as many existing allometric equations as possible, intending to better link field LiDAR estimates, and that the reasoning behind each estimation would be more intuitive. The RMSE for DBH estimation was 7.1 cm and 28% of mean, which undoubtedly had a large effect on volume and carbon predictions.

As model estimates (such as DBH or species) were input variables of subsequent models, errors were likely confounded, which may explain the relatively high RMSEs for above-ground volume and carbon stocks (87% and 74% of the means, respectively). LiDAR-derived height underestimates are considered a common source of error (Hayashi et al. 2014), and indeed such underestimates may have contributed slightly to the above noted error; however, we feel that, at 21pts/m², the LiDAR was of sufficiently high density to capture crown apices, suggesting that this source of error may have been minimal relative to others. To this point, we did not note consistent negative biases in volume or carbon at the tree level that would be expected given the equations used, had heights been underestimated. We believe the majority of error in each of the tree estimates could be attributed to tree crown segmentation errors (which influenced crown metrics used to estimate stem DBH), such as crown edge clipping and inclusion of neighboring tree crowns. We suspect that more spatially uniform trees (both in terms of horizontal and vertical strata) and improvements to the layer stacking algorithm would lead to better crown delineation, and thus better estimates of stem diameter, such as those

made by Popescu et al. (2003) or Yu et al. (2011) who reported 18% and 10% RMSE of average DBH respectively. Overall, little work has been done to incorporate tree-level analyses of LIDAR data into operational forestry, so it remains to be seen what tolerance for error there may be in practice.

Each of the three plot-level estimates (basal area, volume, and carbon stock) had considerably greater accuracy when compared to the tree-level estimates. The additive method consistently underestimated plot attributes by an average of 8-11%, which has always been a challenge for the ITC approach simply due to undetected trees (Hyypä and Inkinen 1999, Yu et al. 2010). Because small trees are most commonly missed in segmentation, Maltamo et al. (2004) attempted to correct for these omissions by using hypothetical diameter distributions to fill in the missing data. Others have attempted similar modeling approaches (REFS), which add a considerable amount of complexity to the predictions. We chose to correct the predictions by simply adding the percentage associated with omission and subtracting the percentage of commission errors. This approach yielded far higher r-squared values, lower RMSE, and a very low mean bias when compared to the uncorrected additive method. Initially this was done on a plot-by-plot basis, as commission and omission were known for each individual plot. However, because these errors are rarely available, this approach was deemed impractical. Instead, we used the mean commission and omission for each forest type for the correction, at the cost of slightly reduced accuracy (by several percent) in predictions. Collecting these error values in generalized forest types requires little field effort, and these values could presumably be used at similar sites, indicating that the field effort required may be less than that needed for developing models for the AB approach. We note that even without

the aforementioned corrections, the uncorrected additive approach produced estimates of basal area, volume, and carbon stock (17%, 20%, and 21% RMSE, with an average underestimate of 11%, 8%, and 10% respectively) that may be acceptable for particular operational inventories.

The AB volume estimates were also compared to the field measurements on a plot level, and yielded a considerably lower r-squared, higher RMSE, and stronger bias, in comparison with the ITC approach. Thus, in this study, both the corrected and uncorrected ITC approaches produced estimates of basal area, volume, and carbon with greater accuracy than those from the AB approach. One possible explanation for this finding is the age of the training data used for the AB model calibration, which was on average five years older than the LiDAR data. Though growth modeling was used to update tree sizes to account for this five-year lag, this update admittedly introduced uncertainty. Curiously, the out-of-bag r-squared was considerably higher than the r-squared from the simple regression using withheld plots, perhaps confirming a suspected difference between the older training and the newer validation data. A direct comparison between AB and corrected ITC methods yielded r-squared and RMSE values similar to the AB *vs.* field comparison, indicating that little consistent disagreement exists between LiDAR and the field data that may have been introduced (for example, where plot centers misaligned). One important contrast between the two approaches is that ITC delineation takes considerably more computing time than the AB approach. In this instance layer stacking took many times the computational effort than did the random forest prediction. Thus, any benefits of the ITC approach such as accuracy or tree level information, must be weighed against the additional computation time required.

Stand level analysis indicated reasonable agreement with the AB approach. Once again, the AB approach produced a slight overestimate compared to the ITC approach, with a 5% difference on average. The ITC approach only used trees >2m distance from the border of the stand, so as to prevent clipping and inclusion of trees from the adjacent stand. Similarly, the ITC approach only included 10 x 10m blocks that were entirely within the stand, thus discounting blocks that were split between two stands. Although at a stand level both of these edge effects were likely trivial, they may help account for some of the difference in performance (6% RMSE) between the two approaches. Overall, given this level of agreement, we conclude that both the corrected ITC approach and the AB approach can be used interchangeably at a stand level.

Conclusion

In summary, this paper demonstrates the effectiveness of the layer-stacking individual tree approach, for estimating some of the most important forest biometrics across a tree-, plot-, and stand-levels using LiDAR data. In doing so we have introduced several novel methods for measuring individual tree point clouds from LiDAR data. These include quantifying pointiness, the use of first-order differences, measuring ground points beneath the tree, and correcting for segmentation errors in crown width. We have also demonstrated species level classification using only LiDAR and illustrated a potential benefit of having multiple LiDAR flights from different seasons and with different machines for comparing intensity values. Finally, we have improved plot level estimates using an individual tree crown method, as compared to an area-based method, which indicates that the additional information derived by separating tree crowns is not just of value by itself at the tree level, but aids in the accuracy of larger analyses. Though

the benefits of individual tree methods must be weighed against increased computation time, we feel that as computing power continues to improve and practitioners find new ways of using individual tree data, the future of individual tree delineation will be a positive one.

CHAPTER THREE:
THREE-DIMENSIONAL POINT CLOUD RECONSTRUCTUION FROM
AERIAL PHOTOS AS A MEANS OF ESTIMATING INDIVIDUAL TREE
HEIGHT IN CONIFER STANDS

Introduction

Accurate forest canopy measurements are needed for a wide range of forestry and ecological purposes. However, measuring and characterizing canopy structure using traditional methods is challenging, given the difficulty of direct measurements. Obtaining accurate individual tree heights in particular has long posed a challenge for forest inventories, regardless of the method employed. This challenge has led to estimates of height being derived from stem diameter at breast height, or generalized area-based methods describing general canopy height, both of which have innate inaccuracies.

Individual tree heights can be obtained by a variety of inventory methods. In the field, devices such as clinometers or laser hypsometers are typically used (Wing et al. 2004). In practice, the accuracy of these ground-based measures is compromised in closed-canopy forests where individual tree tops are difficult to discern. Further, ground-based methods are labor intensive and are thus applied to a relatively small subsample of trees. From the air, digital stereo-photogrammetry is often used to estimate heights by quantifying the parallax between two images. High resolution photographs with precise overlap are required for this method, and information from only two images at a time can be used. Recently, airborne Light Detection And Ranging (LiDAR) has gained popularity for characterizing forest canopy structure, including tree heights, from a three-dimensional point cloud (Næsset and Økland 2002). As LiDAR imagery becomes more

readily available, and with costs decreasing and point density increasing, it is becoming more widely accepted as the standard for characterizing forest canopy structure, particularly over large remote areas, such as Alaska (Wulder et al. 2012).

Despite its promise as a forest inventory tool, LiDAR has several drawbacks. First, its accuracy strongly depends on pulse density. In order to obtain the resolution required to capture conifer apices (5 pulses per meter [ppm] or greater in our experience), flight lines currently must be close to the ground or must have considerable overlap. As of 2015, LiDAR imagery of this resolution tends to be cost-prohibitive for most potential users. Although lower resolution LiDAR is often freely available through various government agencies in the U.S. and Canada, this resolution (usually 1-3 ppm) may be too low to reliably predict individual tree heights without accounting for a negative bias or creating a predictive model.

An emerging photogrammetric method known as *structure-from-motion* (SfM) may provide a cost effective alternative to LiDAR for generating a canopy surface model, which is a computerized height maps of the forest canopy, used to measure absolute height of trees above ground. The SfM method relies on readily available software that utilizes multiple overlapping aerial digital photographs to produce a three-dimensional point cloud similar in many ways to LiDAR. Like LiDAR, the images or SfM point clouds must be geo-referenced and aligned either using ground-truth data or other remote sensing utilities. Although the concepts underlying SfM have been in use since the early 1990s, former computational restrictions have limited their widespread use. The field of archeology has begun using SfM to characterize three-dimensional structures ranging from small artifacts (Samaan et al. 2013) to entire sites (Verhoeven 2011). The field of

geology also has applied SfM to mapping river beds (Javernick et al. 2014) and topographic structure (Fonstad et al. 2013).

To date, SfM forest applications have addressed larger-scale area based inventories and have been conducted in conjunction with LiDAR (White et al. 2012). One potential limitation in using standard LiDAR techniques to obtain area-based estimates from photogrammetric point clouds (Pitt et al. 2014) is that model calibration and intense ground sampling may be required with each new data acquisition. Canopy metrics used for area-based LiDAR estimates often include mean canopy height, minimum height, standard deviation, histogram analysis, and other characteristics that vary greatly depending on canopy penetration of the laser pulses. Time of day and light level will change the depth to which SfM point clouds can penetrate canopies, thus altering these metrics from one acquisition to the next. However, individual tree height and other direct tree measurements will be less subject to change. For example, Lisein et al. (2013) made limited individual tree measurements using near-infrared photographs.

However, one known limitation of SfM is its inability to penetrate dense forest canopies, meaning that, unlike LiDAR, it can be difficult to produce digital elevation models (DEMs; i.e., ground surface topography) where bare ground is not visible. Accurate DEMs are needed to estimate individual tree heights by subtracting the canopy surface from the ground. To overcome this limitation, we have merged SfM data (point clouds characterizing canopy structure) with commonly available low-resolution LiDAR data (sufficient to derive a DEM), producing a relatively low-cost alternative to high-resolution LiDAR-derived canopy surface models. However, in forests with rather sparse canopies, SfM may function as a stand-alone product, with a basic DEM being generated

from ground points visible through canopy interstices. To enhance our ability to derive a DEM from SfM point clouds, we used color infrared imagery to spectrographically filter out vegetation and highlight these interspersed ground points prior to more standard ground point classification by height filtering, which to the best of our knowledge represents a novel workflow.

Our objective was to evaluate the efficacy of SfM imagery – either as a replacement or as a supplement to more traditional methods – for estimating tree heights by testing it against field-measured heights, digital stereo photo interpretation, and LiDAR height estimates of individual trees. Our results demonstrate that SfM shows promise as an additional low-cost forest inventory method, with potential to be used over large areas on a frequent return interval (e.g., five years), provided the terrain is flat, bare earth is visible, or a LiDAR DEM is used in conjunction.

Methods

Efficiently meeting our objective required that we locate a site that had existing field-measured tree heights, high resolution aerial photographs, and LiDAR data. Together these data sets permitted the comparison of tree heights estimated by five methods: field-measured with hypsometer (henceforth FIELD), digital stereo-photo interpretation (DSI), LiDAR, SfM using the LiDAR DEM (SfM-LDEM), and SfM using a DEM derived from the SfM photographs themselves (SfM-SDEM).

We selected a study site within the US Forests Service’s Penobscot Experimental Forest in central Maine, U.S.A. Ground-based height measurements had been obtained on dozens of 16-m fixed radius permanent plots. We selected 15 plots from four stands for measurement, each stand being part of a long-term study on selection harvests, and thus

having a multi-aged canopy structure. Stand were dominated by *Picea rubens* (red spruce), *Abies balsamea* (balsam fir), and *Tsuga canadensis* (eastern hemlock). The four stands spanned a range of structural characteristics, with stem densities ranging from 351 to 558 stems ha⁻¹ and basal areas from 7.9 to 33.6 m² ha⁻¹ (Table 3.1). Tree heights and locations (azimuth and distance from plot centers) were recorded in the field by US Forest Service personnel between Spring of 2011 and Summer of 2013 using *Haglöf Vertex III ultrasonic hypsometers*.

Table 3.1. Summary statistics for each species measured. Diameter at breast height in centimeters (DBH) and height in meters (Ht) by species and measurement method (SD = standard deviation) across each of the four stands measured.

	Mean \pm SD	Min.	Max.
<i>Abies balsamea</i> (n=27 trees)			
Stem DBH	20.2 \pm 4.0	11.7	28.2
FIELD Ht	17.27 \pm 1.89	12.37	21.06
LiDAR Ht	16.42 \pm 1.62	12.42	19.44
SfM-LDEM Ht	15.93 \pm 2.06	10.93	20.21
SfM-SDEM Ht	15.78 \pm 1.99	11.96	18.64
DSI Ht	15.69 \pm 3.69	9.08	24.99
<i>Tsuga canadensis</i> (n=43 trees)			
Stem DBH	36.4 \pm 4.1	12.2	58.2
FIELD Ht	19.46 \pm 3.31	10.03	24.32
LiDAR Ht)	18.96 \pm 3.19	9.48	24.24
SfM-LDEM Ht	19.55 \pm 3.43	10.67	25.50
SfM-SDEM Ht	19.71 \pm 3.63	9.78	25.02
DSI Ht	18.86 \pm 3.66	10.82	26.79
<i>Picea rubens</i> (n=39 trees)			
Stem DBH	32.1 \pm 3.7	13.0	48.5
FIELD Ht	19.74 \pm 3.04	11.86	25.91
LiDAR Ht	18.88 \pm 2.90	10.64	24.56
SfM-LDEM Ht	19.15 \pm 3.08	12.34	25.45
SfM-SDEM Ht	19.02 \pm 3.40	13.07	26.01
DSI Ht	18.87 \pm 3.41	11.21	24.99

Note: FIELD=field-measured with hypsometer, DSI=digital stereo-photo interpretation, SfM-LDEM=structure-from-motion (SfM) using the LiDAR DEM, SfM-SDEM=SfM using the SfM DEM.

Color infrared aerial photos were flown covering the experimental forest in late 2013 in leaf-off conditions. For this reason we have focused our analyses on conifers. Photos were taken with a Canon EOS Rebel T2i DSLR adapted for near-infrared acquisition, flown at an altitude of approximately 1,220 meters above ground at a resolution of approximately 14 cm per pixel, with 60 % endlap and 40 % sidelap. These photos were used for both digital stereo-photo interpretation and SfM analyses. Digital stereo-photo interpretation was done by a trained interpreter in ERDAS Imagine 2014

with the Stereo Analyst version 14.0 application (ERDAS Inc. 2014). Plots were analyzed individually by selecting the appropriate digital stereo-model for display within the Digital Stereoscope workspace, and individual heights were obtained for each preselected tree with the 3D Measure tool.

LiDAR was flown in late October of 2013 in leaf-off conditions at an average resolution of 6 ppm. A full waveform Riegl LMS-Q680i was used with a pulse rate of 150 Khz. Footprint size was on average 0.17 m. Altitude was approximately 600 m above ground. Ground points were classified by the LiDAR service provider.

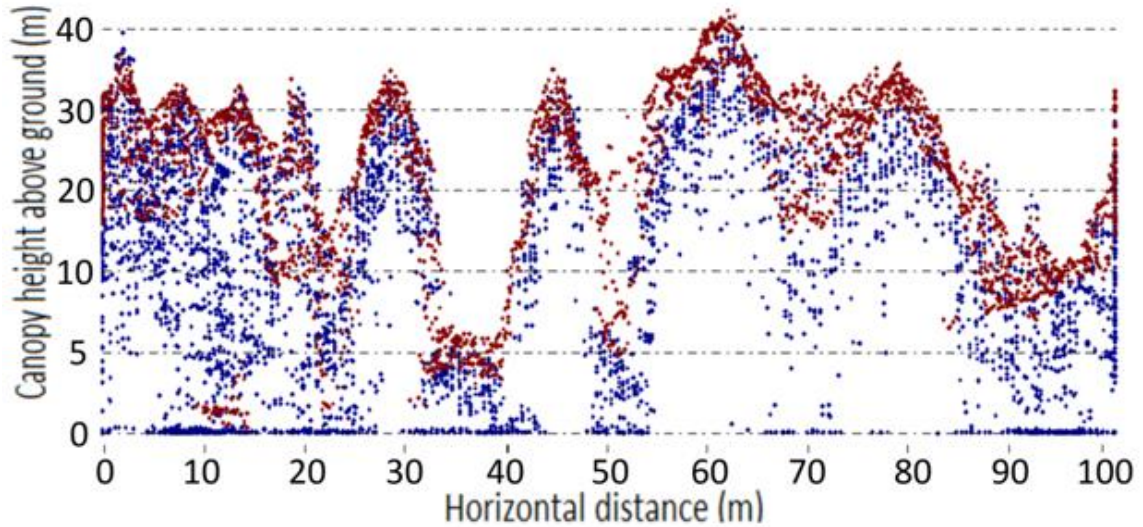
The SfM reconstruction was processed using Agisoft Photoscan software (AgiSoft LLC, 2011). SfM can best be defined as a series of steps that consist of calibrating for the camera's lens distortion automatically, identifying common points within photos, determining camera positions in space based on differing orientations of those points, refining those positions through a bundle adjustment cost function, and then reconstructing fine structures between those points using somewhat more typical stereo methods such as semi-global matching.

The SfM reconstruction was geo-referenced by aligning it to the already well-referenced LiDAR dataset using the open-source program CloudCompare (Cloud Compare, 2011), which automatically determines scale and transformation using an iterative closest-point algorithm, as well as with manual refinement where necessary. Over large spatial scales, the two point clouds were difficult to align, likely due to small inconsistencies in the photo reconstruction that multiplied with increasing distance from the alignment control points. Therefore, the SfM point cloud was separated into segments of roughly 500 m on each side to establish fresh control points. The trees measured were

not used in the alignment process, and attempts were made to use anthropogenic features (e.g., buildings, roads) for alignment before resorting to trees.

Because the point-cloud data (LiDAR and SfM) were measured as height above sea level, and thus would incorporate hills and terrain changes into elevation, they were normalized, creating a canopy height model so as to only measure height above ground (Fig. 3.1). Thus, for both the LiDAR and the combined LiDAR-SfM model (SfM-LDEM), the digital elevation model (DEM) used to obtain absolute tree height originated from the LiDAR ground points. In the case of the SfM stand-alone model (SfM-SDEM), the DEM originated from the SfM photos alone. This DEM was generated by first spectrographically filtering points with high infrared reflectance to remove vegetation, then using a height filtering algorithm within the BCAL software package (BCAL LiDAR Tools, 2014), and finally interpolating with inverse distance (Streutker and Glenn 2006). Individual tree height measurements were estimated by manually locating tree top in the point cloud for both the LiDAR and SfM data, with the highest point on the crown taken as it's apex.

Figure 3.1: A structure from motion point cloud (red) overlaid on top of a LiDAR point cloud (blue). Both point clouds have been normalized against the LiDAR-derived DEM, showing height above ground. Note that the two point clouds are nearly identical at the canopy surface; however, LiDAR penetrates the canopy and thus better depicts sub-canopy structure and ground.



Height was determined for a total of 109 trees with all five measurement types.

Digital stereo-photo manual measurement was the greatest limiting factor, as the interpreter could only resolve individual heights for this subset of trees. To determine if the five measurement methods produced similar tree heights, we first employed a linear mixed-model ANOVA, testing if height was influenced by measurement type, species, and the interaction between the two. To account for the hierarchical data structure (trees nested within plots, plots nested within stands), these variables were included in the model as random nested effects. This model initially included stem diameter as a covariate to account for differences in trees size among species (balsam-fir tended to be shorter than the others); however, this did not improve the model, and was thus left out of the final model. Results from this preliminary analysis revealed a significant interaction between species and method ($P = 0.01$), which precluded the testing of the main effect of measurement type across species, the original purpose of our study. For this reason, we

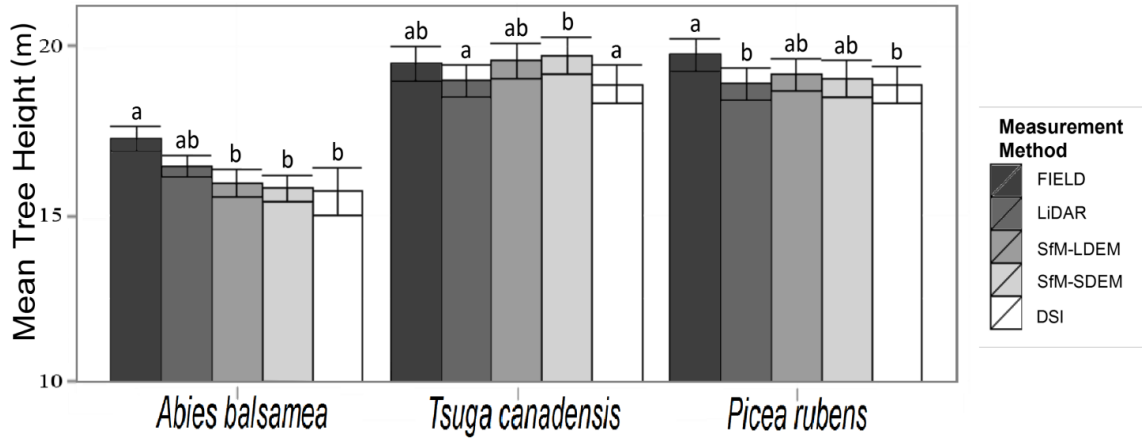
performed separate linear mixed-model ANOVAs for each of the three species, allowing us to examine the effect of measurement type. These ANOVAs included the random effects mentioned above. Post-hoc comparisons of least square means were made using Tukey's test (at $\alpha=0.05$) to test for differences among measurement types.

In order to assess bias and precision of each measurement type we used the mean height of all five measurement types obtained for each tree (within a species) as a reference. We define bias as the mean of the differences between each observation and the reference, and precision as the mean of the absolute values of these differences.

Results and Discussion

All three ANOVAs (one per species) revealed statistically significant differences among the measurement types (Fig. 3.2). Though results varied by species, several general trends emerged. For example, LiDAR and SfM-LDEM height estimates did not differ significantly from one another with a mean difference of 0.21 ± 1.29 m (mean \pm SD); however, SfM-SDEM differed significantly from LiDAR for *Abies balsamea*, with SfM-SDEM 0.64 ± 1.73 m lower than LiDAR measurements. SfM-SDEM never differed significantly from SfM-LDEM ($p < 0.05$). DSI and FIELD measurements differed significantly for *Abies balsamea* and *Picea rubens*, with DSI underestimating height by an average of 0.86 ± 1.99 m in both species; FIELD produced the tallest estimates in these same species, and DSI consistently produced the lowest height measurements and the greatest variation among estimates (Table 3.1). In no instance did one single measurement method differ significantly from all others, nor did both SfM methods differ significantly from all the traditional methods.

Figure 3.2: Mean tree height by species and measurement method. Values with different letters (within a species) are significantly different (Tukey’s test at $\alpha < 0.05$). Error bars indicate standard deviation. FIELD=field-measured with hypsometer, DSI=digital stereo-photo interpretation, SfM-LDEM=structure-from-motion (SfM) using the LiDAR DEM, SfM-SDEM=SfM using the SfM DEM.



The species by measurement type interaction noted in our preliminary analysis may have arisen from *Abies balsamea* being considerably shorter than other species, suggesting that not all measurement types performed equally on shorter trees. Alternately, different canopy structures among species may have led to misidentification of tree apices by one or more methods.

The bias and precision for each measurement type and species combination can be seen in Table 3.2. Despite statistically significant differences among measurement types revealed by the ANOVAs (above), many of these differences were small enough to have little impact operationally. DSI had consistently high bias and low precision when compared to other methods tested. Bias and precision of SfM-LDEM was often on par or better than those of LiDAR, with directional bias not exceeding 0.28 m. Directional bias of the SfM-SDEM measurement method did not exceed 0.44 m.

Table 3.2: Mean biases and absolute differences between measurement methods. These were used to assess bias and precision respectively.

Method	<i>Abies balsamea</i>		<i>Tsuga canadensis</i>		<i>Picea rubens</i>	
	Bias (m)	Absolute difference (m)	Bias (m)	Absolute difference (m)	Bias (m)	Absolute difference (m)
FIELD	1.05 ± 1.15	1.31	0.15 ± 0.87	0.07	0.60 ± 0.79	0.77
LiDAR	0.20 ± 0.74	0.65	-0.35 ± 0.63	0.59	-0.25 ± 0.87	0.65
SfM-LDEM	-0.28 ± 1.48	1.10	0.24 ± 0.61	0.52	0.02 ± 0.71	0.55
SfM-SDEM	-0.44 ± 1.49	1.17	0.40 ± 1.35	1.04	-0.11 ± 1.35	1.06
DSI	-0.53 ± 2.31	1.77	-0.45 ± 1.66	1.37	-0.26 ± 1.70	1.34

Note: FIELD=field-measured with hypsometer, DSI=digital stereo-photo interpretation, SfM-LDEM=structure-from-motion (SfM) using the LiDAR DEM, SfM-SDEM=SfM using the SfM DEM.

Precision was notably lower in the SfM-SDEM and DSI measurements, when compared to other methods, which may be attributable to differing canopy closure. That is, stands with greater canopy stratification or leaf-off deciduous trees tended to provide more accurate SfM-DEMs simply because more ground was visible in the photos. In these cases SfM alone is likely sufficient for tree height measurements. However, in many instances, there were sizable areas without ground points, possibly resulting in elevation changes being missed, thereby creating uncertainty in tree heights. Using higher resolution photos or photos taken closer to midday when the sun is directly illuminating canopy interstices would likely have improved SfM-SDEM measurements. As noted by White et al. (2012), an analysis of SfM efficacy in different forest types is required; this paper illustrates SfM's effectiveness in heterogeneous softwood stands. More work is

needed, however, to determine the image resolution, percent canopy closure, topographic smoothness of the site, and flight parameters required for SfM to work effectively as a stand-alone product.

In many instances, combining SfM reconstructions with a LiDAR DEM will yield more reliable tree height measurements, simply because LiDAR pulses penetrate the canopy and thus yield more ground points. In our study site, the terrain was relatively flat, which permitted a reasonable interpolation between sparse ground points in the SfM-derived DEM; in rougher terrain, this interpolation may be unreliable. Existing DEMs can be obtained from LiDAR data that may be too coarse or too old to yield height measurements. Used in this manner, SfM may offer a low-cost alternative to flying LiDAR repeatedly or at high resolutions, as noted by Pitt et al. (2014). We note, however, that geo-referencing SfM to the DEM must be done with great care to ensure that scale has been properly assigned, since small differences in scale between the point cloud and DEM can accumulate over large areas.

We note that we did not attempt to correct for camera parameters or lens distortion in our SfM data, which may partly explain the inconsistencies in the DEM mentioned above. Instead, we overcame this limitation by spatially sub-setting the SfM point cloud and georeferencing these subsets individually. We believe this approach is sufficient when analyzing point clouds at the level of individual trees or forest stands, given the recent advances in software. Such an approach was not necessary with the stand-alone SfM, because tree height was measured relative to the ground directly beneath it, and landscape-level inconsistencies between the SfM-SDM and LiDAR DEM had no measurable impact on individual tree heights.

Flight parameters needed for SfM are also considerably less restrictive than those of traditional aerial photos. Given SfM's success with different camera angles in the past (De Reu 2013), it is likely that oblique photos taken from differing altitudes would serve as well, if not better, for reconstruction provided photos share enough points for semi-global matching. Greater change in perspective would better reveal areas otherwise obscured in a top-down view, thereby improving reconstructions. One final benefit of SfM is that its point clouds are inherently colored, as opposed to LiDAR, which usually require color to be added afterwards from photos flown during a different acquisition, due to differing flight parameters between LiDAR and aerial photos. This benefit facilitates species and object detection by eye and by spectrographic filtering. In this instance, we believe the DEM generation from images was aided significantly by the near infrared band, which allowed us to easily remove vegetation prior to processing.

Our findings suggest that SfM reconstructions can serve as a low-cost supplement to, or in some cases, replacement for, LiDAR or more traditional aerial digital stereophotographs in studies of forest structure. However, because SfM cannot penetrate the forest canopy, it cannot resolve detail on sub-canopy structures or covered ground points, as can LiDAR. As shown here, it can provide canopy-surface and tree-height data comparable to that of LiDAR. As such, it could lend itself well to the delineation of individual tree canopies (i.e., segmentation, see Kwak et al. 2007) using methods commonly applied to LiDAR point clouds. Further, because it inherently includes spectral information, it can be used to resolve tree species, as is done with traditional aerial photographs (Gougeon 1995). SfM could therefore serve as an invaluable tool with potential widespread usage in forest inventories and studies of forest canopy structure.

EPILOGUE

Summary of Chapters

For many decades, forest inventories have benefited from remote sensing data. In recent years, thanks to technological advancements in photogrammetry and laser range finding, researchers and managers have had access to forest structure data in the form of three-dimensional point clouds, that is, dense clusters of spatially explicit points that represent the structure of the forest canopy. Metrics derived from these point clouds have proven invaluable for estimating forest biometrics, such as biomass (Zolkos et al. 2013), tree density (Næsset and Bjercknes 2001), height, and stem diameter (Means et al. 2000). Most of these metrics, however, are of a coarse nature, and are derived from secondary height characteristics obtained on a per-area basis, and thus depict structure at the level of forest plots or stands. However, direct measurements of individual tree attributes, visually evident in high resolution point clouds, could be of benefit by providing tree lists which could then be used for more precise management, and more intuitive inventories. The above work establishes methods by which detailed individual tree attributes can be extracted from high resolution point clouds.

Chapter I detailed a new algorithm by which individual tree shapes can be isolated from a larger LiDAR point cloud, a process referred to as *segmentation*. Existing algorithms typically use the rise and fall of tree canopies on the canopy surface to detect the tree outline, then isolate anything within that outline. These so-called watershed algorithms are ineffective at isolating overtopped trees beneath a closed canopy, at isolating trees whose canopies are tightly interlocked (often deciduous species), and at

isolating the structure of a tree without including objects that lie beneath it. Because of these limitations, tree detection rates remain quite low even with the highest quality LiDAR (Vauhkone et al. 2011). The layer stacking algorithm presented in Chapter I (known as layer stacking), uses a series of horizontal layers to detect tree structure throughout the entire forest strata, rather than just the surface. Results demonstrated that layer stacking performed on par or better than watershed delineation in nearly every forest stand type examined, with the greatest improvements observed in deciduous stands, which have traditionally been difficult to segment.

Chapter II applied the layer stacking segmentation algorithm presented in Chapter I to the task of deriving metrics to estimate stem diameter, stem volume, aboveground biomass, and carbon content of each tree in the forest over 10 cm diameter. These estimates can then be summed to obtain plot and stand level estimates on a per-area basis. The process begins by classifying segmented trees by species, using several measures of canopy shape and infrared reflectance. Next, stem diameter was estimated using height, canopy width variables, and species as predictors. Estimated diameter and tree height was then used to estimate bole volume using local taper equations. Stem volume was converted to biomass from density equations, and leaf and branch biomass was estimated from diameter using local weight tables. Finally, biomass was converted to carbon content using biomass to carbon specific density equations. Each of the three metrics of interest (diameter, volume, and carbon stock) were compared to field values at a tree and plot level. Finally, the individual tree method was compared to the coarser area based method mentioned above. Results indicated that the extra information of measuring each tree lead to superior estimates on a plot level. Thus, we conclude that measuring

individual trees yields not only more detail, but more accuracy than traditional area based point cloud interpretation.

Finally, Chapter III evaluated a new alternative for generating dense point clouds from photogrammetry, known as *structure-from-motion* (SfM). This method of point cloud reconstruction is considerably more cost effective than the more traditional alternative, LiDAR, which has often been prohibitively expensive to foresters. Similar to LiDAR, most work with photogrammetric point clouds has focused on area-based estimates (Bohlin et al. 2012, White et al. 2013). However, with imagery of a high enough resolution, individual tree crowns can be observed and measured. To illustrate this concept, individual tree height measurements were made using SfM alone and SfM in conjunction with LiDAR, and then a comparison was drawn between these and field measurements, LiDAR measurements, and digital stereo-photogrammetry measurements. Results revealed little difference between the various methods, suggesting that SfM may be a suitable alternative or supplement to LiDAR for forest inventories, particularly those that need to be flown repeatedly and at low cost.

The Future of Point Cloud Technology

Technological advancements in this new field of three-dimensional measurement show little sign of slowing down, so the new methods presented here will be essential for taking full advantage of the advancements in data acquisition expected in the coming years. There have been several stages of development in LiDAR's history, starting with single profile LiDAR which measured only a two-dimensional profile, then moving to discrete return LiDAR which measured three dimensions but could not penetrate trees

and measure multiple points vertically, and finally leading to the full waveform LiDAR common today, which is able to detect multiple points throughout the tree canopy and create robust three dimensional point clouds. There is however, every indication, that we may be entering a new stage thanks to the advent of single-photon-LiDAR (SPL). SPL is an order of magnitude faster than full waveform, because while full waveform sends out one beam of light at a time, SPL splits the beam into many pieces and sends out at least 100 beams at once. This is possible because a SPL detector is capable of receiving as little as one photon of light as a hit, and thus can be considerably faster in the collection of new points than full waveform LiDAR which requires a continuous stream of light to register a new point. The result is a point cloud of a high enough resolution to detect individual trees, at a fraction of the cost of traditional low resolution LiDAR.

Another recent development in point cloud generation is multispectral LiDAR. While traditional LiDAR sends out a single infrared beam of light, multispectral LiDAR sends out several beams at different wavelengths. One can then examine the intensity that each of those beams was returned at, and assign a color value to each three dimensional point in the point cloud. Multispectral LiDAR would help foresters in several ways: it would aid in segmentation since trees next to one another are often different colors, it would help with species identification because each species often has a unique spectral reflectance, and it would aid in assessing tree health, leaf area, and live crown, since normalized difference vegetation indices could be made for each tree at a three dimensional level.

Finally, point clouds generated from SfM will likely become more ubiquitous. Concurrently, SfM point clouds are best used in conjunction with a LiDAR elevation

model, serving as a cheap means of reassessing forest attributes rather than flying LiDAR again. As more public LiDAR is flown, more areas will become open to SfM analyses. Due to differences in SfM point clouds stemming from different flight parameters, such as time of day, and cloudiness, it has been difficult to apply traditional area-based approaches to SfM point clouds. This has made the development of regional models, like those developed with LiDAR, very difficult. Thus, there has been little operational use of SfM for forest analytics. This will likely change as scientists find new ways to interpret SfM point clouds, and as individual trees are measured, rather than area-based metrics.

Thus the future of individual tree analysis is a bright one, with multiple lines of technology leading to improved individual tree analytics. With each and every tree in the forest quantified, it will fall upon the next generation of foresters and scientists to make the best use of these tremendous datasets.

REFERENCES

- AgiSoft LLC, 2011. Version 1.0.4. Standard Edition, Agisoft PhotoScan. Available from <http://www.agisoft.ru/products/photoscan/> [accessed October 2014].
- Asner, G. P., Knapp, D. E., Kennedy-Bowdoin, T., Jones, M. O., Martin, R. E., Boardman, J., & Hughes, R. F. (2008). Invasive species detection in Hawaiian rainforests using airborne imaging spectroscopy and LiDAR. *Remote Sensing of Environment*, 112(5), 1942-1955.
- BCAL LiDAR Tools, 2014 Version 1.5.3. Idaho State University, Department of Geosciences, Boise Center Aerospace Laboratory (BCAL), Boise, Idaho. Available from <http://bcal.geology.isu.edu/envitools.shtml> [accessed October 2014].
- Brandtberg, T., Warner, T. A., Landenberger, R. E., & McGraw, J. B. (2003). Detection and analysis of individual leaf-off tree crowns in small footprint, high sampling density lidar data from the eastern deciduous forest in North America. *Remote sensing of Environment*, 85(3), 290-303.
- Brandtberg, T. (2007). Classifying individual tree species under leaf-off and leaf-on conditions using airborne lidar. *ISPRS Journal of Photogrammetry and Remote Sensing*, 61(5), 325-340.
- Breidenbach, J., & Astrup, R. (2014). The semi-individual tree crown approach. In *Forestry applications of airborne laser scanning* (pp. 113-133). Springer Netherlands.
- Breidenbach, J., Næsset, E., Lien, V., Gobakken, T., & Solberg, S. (2010). Prediction of species specific forest inventory attributes using a nonparametric semi-individual tree crown approach based on fused airborne laser scanning and multispectral data. *Remote Sensing of Environment*, 114(4), 911-924.
- Bucksch, A., Lindenbergh, R., Abd Rahman, M.Z., & Menenti, M. (2014) Breast height diameter estimation from high-density airborne LiDAR data. *Geoscience and Remote Sensing Letters, IEEE*, 11, 1056-1060.
- Chen, Q. (2007) Airborne lidar data processing and information extraction. *Photogrammetric Engineering and Remote Sensing*, 73, 109.
- Chen, Q., Baldocchi, D., Gong, P., & Kelly, M. (2006) Isolating individual trees in a savanna woodland using small footprint lidar data. *Photogrammetric Engineering & Remote Sensing*, 72, 923-932.
- Cloud Compare - Point Cloud Analysis Software. 2011. Version 2.5.5.2. EDF R&D and Telecom ParisTech. <http://www.cloudcompare.org/> [accessed June 2014].

- Cook, B.D., Nelson, R.F., Middleton, E.M., Morton, D.C., McCorkel, J.T., Masek, J. G., Ranson, K.J., Ly, L., & Montesano, P.M. (2013) NASA Goddard's LiDAR, Hyperspectral and Thermal (G-LiHT) airborne imager. *Remote Sensing*, 5, 4045-4066.
- De Reu, J., Plets, G., Verhoeven, G., De Smedt, P., Bats, M., Cherretté, B., De Maeyer, W., Deconynck, J., Herremans, D., Laloo, P., Van Meirvenne, M., & De Clercq, W. 2013. Towards a three-dimensional cost-effective registration of the archaeological heritage. *Journal of Archeological Science*, 40(2), 1108-1121.
- Duncanson, L.I., Cook, B.D., Hurtt, G.C., & Dubayah, R.O. (2014) An efficient, multi-layered crown delineation algorithm for mapping individual tree structure across multiple ecosystems. *Remote Sensing of Environment*, 154, 378-386.
- ERDAS Inc. 2014. ERDAS Stereo Analyst User's Guide. ERDAS Inc., Atlanta, Ga.
- Ester, M., Kriegel, H. P., Sander, J., & Xu, X. (1996) A density-based algorithm for discovering clusters in large spatial databases with noise. *Knowledge Discovery in Databases*, 96, 226-231.
- Fonstad, M.A., Dietrich, J.T., Courville, B.C., Jensen, J.L., & Carbonneau, P.E. 2013. Topographic structure from motion: a new development in photogrammetric measurement. *Earth Surface Processes and Landforms*, 38(4): 421-430.
- Gougeon, F.A. 1995. A crown-following approach to the automatic delineation of individual tree crowns in high spatial resolution aerial images. *Canadian Journal of Remote Sensing*, 21(3), 274-284.
- Gupta, S., Weinacker, H., & Koch, B. (2010) Comparative analysis of clustering-based approaches for 3-D single tree detection using airborne fullwave lidar data. *Remote Sensing*, 2, 968-989.
- Harmon, M.E., Woodall, C. W., Fath, B., & Sexton, J. (2008). Woody detritus density and density reduction factors for tree species in the United States: a synthesis.
- Hyypä, J., and Inkinen, M. (1999). Detecting and estimating attributes for single trees using laser scanner. *The photogrammetric journal of Finland*, 16(2), 27-42.
- Javernick, L., Brasington, J., and Caruso, B. 2014. Modeling the topography of shallow braided rivers using Structure-from-Motion photogrammetry. *Geomorphology*, 213, 166-182.
- Kartinen, H., Hyypä, J., Yu, X., Vastaranta, M., Hyypä, H., Kukko, A., Holopainen, M., Heipke, C., Hirschmugl, M., Morsdorf, F., Naesset E., Pitkänen, J., Popescu, S., Solberg, S., Wolf, B.M., & Wu, J. C. (2012). An international comparison of

- individual tree detection and extraction using airborne laser scanning. *Remote Sensing*, 4, 950-974.
- Kim, S., McGaughey, R. J., Andersen, H. E., & Schreuder, G. (2009). Tree species differentiation using intensity data derived from leaf-on and leaf-off airborne laser scanner data. *Remote Sensing of Environment*, 113(8), 1575-1586.
- Koch, B., Heyder, U., & Weinacker, H. (2006) Detection of individual tree crowns in airborne lidar data. *Photogrammetric Engineering & Remote Sensing*, 72, 357-363.
- Koch, B., Kattenborn, T., Straub, C., & Vauhkonen, J. (2014) Segmentation of forest to tree objects. (pp. 89–112) In *Forestry Applications of Airborne Laser Scanning*, Maltamo, M., Næsset, E., Vauhkonen, J., Springer, Netherlands.
- Kozak, A. (2004). My last words on taper equations. *The Forestry Chronicle*, 80(4), 507-515.
- Korpela, I., Ørka, H. O., Maltamo, M., Tokola, T., & Hyypä, J. (2010). Tree species classification using airborne LiDAR—effects of stand and tree parameters, downsizing of training set, intensity normalization, and sensor type. *Silva Fennica*, 44(2), 319-339.
- Kwak, D. A., Lee, W. K., Lee, J. H., Biging, G. S., & Gong, P. (2007) Detection of individual trees and estimation of tree height using LiDAR data. *Journal of Forest Research*, 12, 425-434.
- Lamlom, S. H., & Savidge, R. A. (2003). A reassessment of carbon content in wood: variation within and between 41 North American species. *Biomass and Bioenergy*, 25(4), 381-388.
- Lee, H., Slatton, K.C., Roth, B.E., & Cropper Jr, W.P. (2010) Adaptive clustering of airborne LiDAR data to segment individual tree crowns in managed pine forests. *International Journal of Remote Sensing*, 31, 117-139.
- Li, J., Hu, B., & Noland, T. L. (2013). Classification of tree species based on structural features derived from high density LiDAR data. *Agricultural and forest meteorology*, 171, 104-114.
- Li, R., Weiskittel, A., Dick, A. R., Kershaw, J. A., & Seymour, R. S. (2012). Regional stem taper equations for eleven conifer species in the Acadian region of North America: development and assessment. *Northern Journal of Applied Forestry*, 29(1), 5-14.
- Liaw, A., & Wiener, M. (2002). Classification and regression by randomForest. *R news*, 2(3), 18-22.

- Lindberg, E., Holmgren, J., Olofsson, K., Wallerman, J., & Olsson, H. (2010) Estimation of tree lists from airborne laser scanning by combining single-tree and area-based methods. *International Journal of Remote Sensing*, 31, 1175-1192.
- Lisein, J., Pierrot-Deseilligny, M., Bonnet, S., and Lejeune, P. 2013. A photogrammetric workflow for the creation of a forest canopy height model from small unmanned aerial system imagery. *Forests*, 4(4), 922-944.
- Maltamo, M., Eerikäinen, K., Pitkänen, J., Hyypä, J., & Vehmas, M. (2004) Estimation of timber volume and stem density based on scanning laser altimetry and expected tree size distribution functions. *Remote Sensing of Environment*, 90, 319-330.
- McGaughey, R. J. (2009). FUSION/LDV: Software for LIDAR data analysis and visualization. *US Department of Agriculture, Forest Service, Pacific Northwest Research Station: Seattle, WA, USA*, 123(2).
- Means, J. E., Acker, S. A., Fitt, B. J., Renslow, M., Emerson, L., & Hendrix, C. J. (2000) Predicting forest stand characteristics with airborne scanning lidar. *Photogrammetric Engineering and Remote Sensing*, 66, 1367-1372.
- Morsdorf, F., Meier, E., Allgöwer, B., & Nüesch, D. (2003) Clustering in airborne laser scanning raw data for segmentation of single trees. *International Archives of the Photogrammetry, Remote Sensing and Spatial Information Sciences*, 34, W13.
- Müllner, D. (2013) fastcluster: Fast hierarchical, agglomerative clustering routines for R and Python. *Journal of Statistical Software*, 53, 1-18.
- Naidoo, L., Cho, M. A., Mathieu, R., & Asner, G. (2012). Classification of savanna tree species, in the Greater Kruger National Park region, by integrating hyperspectral and LiDAR data in a Random Forest data mining environment. *ISPRS Journal of Photogrammetry and Remote Sensing*, 69, 167-179.
- Næsset, E. (1997). Estimating timber volume of forest stands using airborne laser scanner data. *Remote Sensing of Environment*, 61(2), 246-253.
- Næsset, E. (2002) Predicting forest stand characteristics with airborne scanning laser using a practical two-stage procedure and field data. *Remote Sensing of Environment*, 80, 88-99.
- Næsset, E., & Bjerknes, K. O. (2001). Estimating tree heights and number of stems in young forest stands using airborne laser scanner data. *Remote Sensing of Environment*, 78(3), 328-340.
- Næsset, E., and Økland, T. 2002. Estimating tree height and tree crown properties using airborne scanning laser in a boreal nature reserve. *Remote Sensing of Environment*, 79(1), 105-115.

- Ørka, H. O., Gobakken, T., Næsset, E., Ene, L., and Lien, V. (2012). Simultaneously acquired airborne laser scanning and multispectral imagery for individual tree species identification. *Canadian Journal of Remote Sensing*, 38(2), 125-138.
- Pitt, D. G., Woods, M., and Penner, M. 2014. A comparison of point clouds derived from stereo imagery and airborne laser scanning for the area-based estimation of forest inventory attributes in boreal Ontario. *Canadian Journal of Remote Sensing*, 40(3), 214-232.
- Persson, A., Holmgren, J., & Söderman, U. (2002) Detecting and measuring individual trees using an airborne laser scanner. *Photogrammetric Engineering and Remote Sensing*, 68, 925-932.
- Peuhkurinen, J., Maltamo, M., Malinen, J., Pitkänen, J., and Packalén, P. (2007). Preharvest measurement of marked stands using airborne laser scanning. *Forest Science*, 53(6), 653-661.
- Popescu, S.C., Randolph H.W., & Ross F.N. (2002) Estimating plot-level tree heights with lidar: local filtering with a canopy-height based variable window size. *Computers and Electronics in Agriculture*, 37, 71-95.
- Popescu, S.C., & Wynne, R.H. (2004) Seeing the trees in the forest: Using lidar and multispectral data fusion with local filtering and variable window size for estimating tree height. *Photogrammetric Engineering & Remote Sensing*, 70, 589-604.
- Popescu, S. C., Wynne, R. H., & Nelson, R. F. (2003). Measuring individual tree crown diameter with lidar and assessing its influence on estimating forest volume and biomass. *Canadian journal of remote sensing*, 29(5), 564-577.
- Rahman, M.Z.A., & Gorte, B.G.H. (2009) Tree crown delineation from high resolution airborne lidar based on densities of high points. In *International Archives of the Photogrammetry, Remote Sensing, and Information Sciences XXXVIII (3/W8)*, Proceedings ISPRS Workshop Laserscanning 2009, Paris, France, September 1-2.
- Rijal, B., Weiskittel, A. R., & Kershaw, J. A. (2012). Development of regional height to diameter equations for 15 tree species in the North American Acadian Region. *Forestry*, 28, 84-91.
- Reitberger, J., Krzystek, P., & Stilla, U. (2008). Analysis of full waveform LIDAR data for the classification of deciduous and coniferous trees. *International journal of remote sensing*, 29(5), 1407-1431.

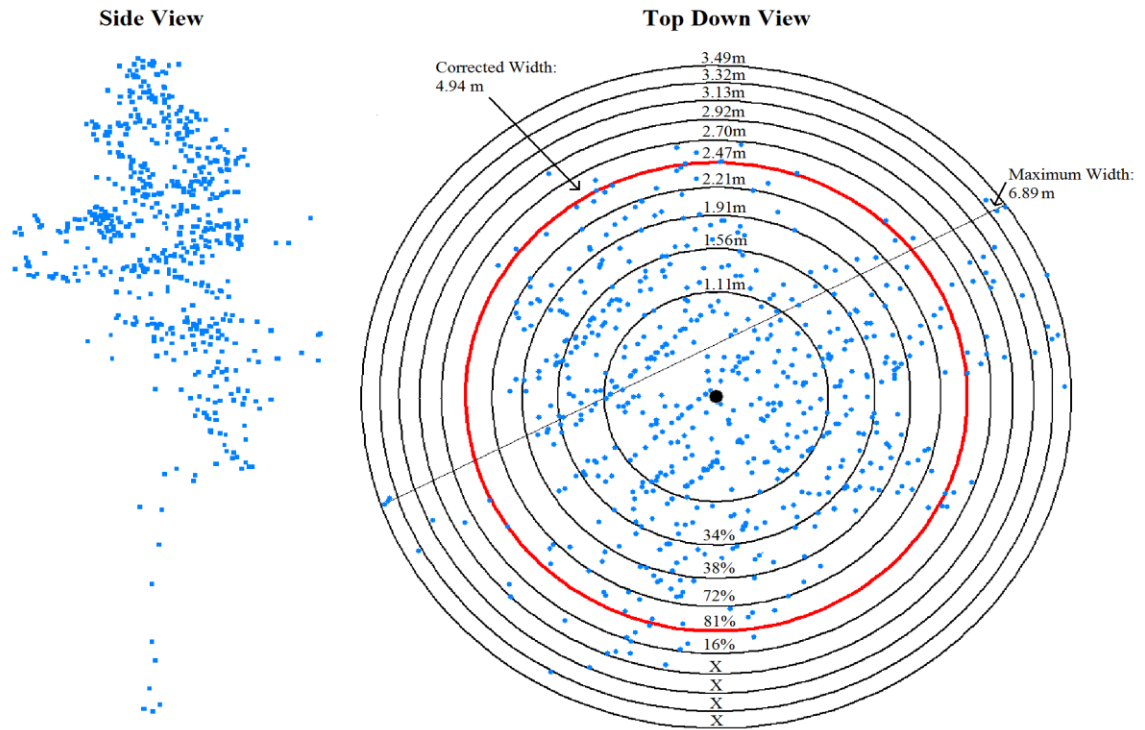
- Reitberger, J., Schnörr, C., Krzystek, P., & Stilla, U. (2009) 3D segmentation of single trees exploiting full waveform LIDAR data. *ISPRS Journal of Photogrammetry and Remote Sensing*, 64, 561-574.
- Russell, M. B., & Weiskittel, A. R. (2011). Maximum and largest crown width equations for 15 tree species in Maine. *Northern Journal of Applied Forestry*, 28(2), 84-91.
- Samaan, M., Raphaële, H., & Pierrot-Deseilligny, M. 2013. Close-range photogrammetric tools for small 3D archeological objects. *International Archives of the Photogrammetry, Remote Sensing, and Information Sciences XL (5/W2)*, 549-553.
- Schäfer, H. (1989). Constructing a cut-off point for a quantitative diagnostic test. *Statistics in medicine*, 8(11), 1381-1391.
- Soille, P. (2009) Segmentation. (pp. 267-274) In *Morphological Image Analysis: principles and applications*. Springer-Verlag, New York, USA.
- Streutker, D.R., & Glenn, N.F. 2006. LiDAR measurement of sagebrush steppe vegetation heights. *Remote Sensing of Environment*, 201(1): 135-145.
- Suratno, A., Seielstad, C., & Queen, L. (2009). Tree species identification in mixed coniferous forest using airborne laser scanning. *ISPRS Journal of Photogrammetry and Remote Sensing*, 64(6), 683-693.
- Vastaranta, M., Holopainen, M., Haapanen, R., Yu, X., Melkas, T., Hyypä, J., & Hyypä, H. (2009) Comparison between an area-based and individual tree detection method for low-pulse density ALS-based forest inventory. *Proceedings of Laser Scanning, Paris, France*, 1-2.
- Vauhkonen, J. (2010). Estimating crown base height for Scots pine by means of the 3D geometry of airborne laser scanning data. *International Journal of Remote Sensing*, 31(5), 1213-1226.
- Vauhkonen, J., Ene, L., Gupta, S., Heinzl, J., Holmgren, J., Pitkänen, J., Solberg, S., Wang, Y., Weinacker, H., Hauglin, K.M., Vegard, L., Packalen, P., Gobakken, T., Koch, B., Naesset, E., Tokola, T., & Maltamo, M. (2011) Comparative testing of single-tree detection algorithms under different types of forest. *Forestry*, 85, 27-40.
- Verhoeven, G. 2011. Taking computer vision aloft—archaeological three-dimensional reconstructions from aerial photographs with PhotoScan. *Archaeological Prospection* 18(1), 67-73.

- Villikka, M., Maltamo, M., Packalén, P., Vehmas, M., & Hyypä, J. (2007). Alternatives for predicting tree-level stem volume of Norway spruce using airborne laser scanner data. *The photogrammetric journal of Finland*, 20(2), 33-42.
- Weiskittel, A., Russell, M., Wagner, R., & Seymour, R. (2012). Refinement of the forest vegetation simulator northeast variant growth and yield model: Phase iii. *University of Maine, School of Forest Resources: Orono, ME, USA*, 96104.
- White, J. C., Wulder, M. A., Varhola, A., Vastaranta, M., Coops, N. C., Cook, B. D., Pitt, D., & Woods, M. (2013). A best practices guide for generating forest inventory attributes from airborne laser scanning data using an area-based approach. *The Forestry Chronicle*, 89(6), 722-723.
- White J.C., Wulder, M.A., Vastaranta, M., Coops, N.C, Pitt, D., & Woods, M. 2013. The utility of image-based point clouds for forest inventory: A comparison with airborne laser scanning. *Forests*, 4(3): 518-536.
- Wing, M.G., Derek, S., & Kellogg, L. 2004. Comparing digital range finders for forestry applications. *Journal of Forestry*, 104(4), 16-20.
- Wulder, M., Niemann, K.O., & Goodenough, D.G. (2000) Local maximum filtering for the extraction of tree locations and basal area from high spatial resolution imagery. *Remote Sensing of Environment*, 73, 103-114.
- Wulder, M.A., White, J.C., Nelson, R.F., Næsset, E., Ørka, H.O., Coops, N.C., Hilker, T., Bater, W.C., and Gobakken, T. 2012. Lidar sampling for large-area forest characterization: A review. *Remote Sensing of Environment* 121, 196-209.
- Yu, X., Hyypä, J., Holopainen, M., & Vastaranta, M. (2010) Comparison of area-based and individual tree-based methods for predicting plot-level forest attributes. *Remote Sensing*, 2, 1481-1495.
- Yu, X., Hyypä, J., Vastaranta, M., Holopainen, M., and Viitala, R. (2011). Predicting individual tree attributes from airborne laser point clouds based on the random forests technique. *ISPRS Journal of Photogrammetry and Remote Sensing*, 66(1), 28-37.
- Young, H. E., Ribe, J. H., & Wainwright, K. (1980). Weight tables for tree and shrub species in Maine. *Maine. Life Sciences and Agriculture Experiment Station. Miscellaneous report (USA)*.
- Zhao, F., Guo, Q., and Kelly, M. (2012). Allometric equation choice impacts lidar-based forest biomass estimates: A case study from the Sierra National Forest, CA. *Agricultural and forest meteorology*, 165, 64-72.

Zolkos, S. G., Goetz, S. J., and Dubayah, R. (2013). A meta-analysis of terrestrial aboveground biomass estimation using lidar remote sensing. *Remote Sensing of Environment*, 128, 289-298.

APPENDIX A

Figure A1: Methods of tree crown measurement. An example of crown width estimation, which was needed to account for segmentation errors resulting in crown overestimates. (1) Concentric rings with equal area are constructed around the center of the tree; (2) The number of points within each ring is tallied; (3) The percent difference from one ring to the next is calculated for all rings containing at least 5% of the total point count (shown below the rings); (4) the radius of the ring with the sharpest percent increase in point count (the red ring) is taken as corrected crown radius.



BIOGRAPHY OF THE AUTHOR

Elias Ayrey was born and raised in Rocky Hill, New Jersey on May 11th, 1990. In 2008 he graduated from Montgomery High School and enrolled at Binghamton University. During his early years at Binghamton, he volunteered at the National Oceanic Atmospheric Administration's Sandy Hook, Howard Marine Laboratory, where he learned he had no taste for small boats in rough seas, and hence might not be an ideal marine biologist.

In his later years as an undergraduate, Elias devoted his time to paleobotany, volunteering at the Binghamton University paleontology department, and making a few significant finds in the field. Elias graduated from Binghamton in 2012 with a Bachelor's degree in science, majoring in Ecology and Evolutionary Biology.

In the fall of 2013 Elias was accepted to the University of Maine as a Graduate Research Assistant in the School of Forest Resources. He soon became fascinated by remote sensing, and LiDAR in particular. During his time at the University of Maine, Elias earned a private pilot license, and aided in several forestry related aerial missions.

Elias is a candidate for the Master of Science degree in Forest Resources from the University of Maine in August 2015.